pH-responsive biopolymer-based supramolecular architectures as biodegradable carriers for DOX delivery

Marzieh Heidari Nia[1,2,3], Said Ashkar[2,3], Jose G. Munguia-Lopez[4,5], Joseph M. Kinsella[5], Theo G.M. van de Ven[2,3*]

[1]Department of Chemistry, College of Science, Shahid Chamran University of Ahvaz, Ahvaz, Iran

[2]Department of Chemistry, McGill University, 801 Sherbrooke Street West, Montreal, QC, H3A 0B8, Canada

[3]Quebec Centre for Advanced Materials (QCAM) and Pulp and Paper Research Centre, McGill University, 3420 University Street, Montreal, QC, H3A 2A7, Canada

[4]Faculty of Dentistry, McGill University, 3640 University Street, Montreal, QC H3A 0C7, Canada

[5]Department of Bioengineering, McGill University, 3480 University Street, Montreal, QC H3A 0E9, Canada

[*]Corresponding author email: theo.vandeven@mcgill.ca

Other authors email:

marzieh.heidarinia@mail.mcgill.ca

said.ashkar@mail.mcgill.ca

jose.munguia-lopez@mcgill.ca

joseph.kinsella@mcgill.ca

Abstract

Cellulose is the most abundant renewable biomaterial on earth and beta-cyclodextrin (βCD) is among the most commonly used biocompatible drug encapsulation agents. Combining these bio-organic materials is a very powerful approach to greatly enhance the bioavailability of many drugs. These systems also allow for optimal selective drug release profiles, high biocompatibility, as well as "green nanomedicine" approaches that are eco-friendly in their synthesis and have minimal ecological toxicity. Herein, we designed a new type of green trifunctional biopolymer-based nanosponge drug carriers polymerized by crosslinking beta-cyclodextrin ethylene diamine (βCD-EDA) with bifunctional hairy nanocellulose (BHNC). In this system, hairy nanocellulose particles is considered as the backbone, and the immobilized cyclodextrin cavities capture the DOX (molecules) via host guest inclusion complexation. BHNC contains aldehyde and carboxyl groups and the latter can react with amino groups in βCD-EDA. Firstly, the crosslinker βCD-EDA was obtained from a simple nucleophilic substitution reaction between beta-cyclodextrin carbonyl imidazole (βCD-CI) and ethylene diamine (EDA). Secondly, BHNC was crosslinked by βCD-EDA through a facile nucleophilic substitution crosslinking reaction of the BHNC activated carboxyl groups by the amine groups on βCD-EDA. We refer to the highly crosslinked polymerized BHNC-βCD-EDA network as BBE. Various ratios of βCD-EDA and BHNC were polymerized with the help of DMTMM as an activator, which resulted in different morphological shapes of BBE, and thus different release profiles and pH-responsiveness were obtained for the BBE polymers. Unlike other polymer-based βCDs and nanosponges, these new types of crosslinked polymer were prepared in a green and safe solvent (water) and with very short reaction times and at room temperatures. Finally, the BBE polymers were tested as biocompatible nanocarriers for controllable doxorubicin (DOX) delivery. These hyper crosslinked polymers show a high capacity for loading DOX with extended DOX release.

Furthermore, breast cancer cell cultures show lower cell viability when DOX was loaded in various BBEs compared to control samples or DOX alone, indicating that our DOX-BBE drug delivery systems are better anticancer agents than DOX alone.

Keywords: biodegradable and biocompatible carriers, liquid crystals, nanosponges, bifunctional hairy nanocellulose, beta-cyclodextrin, hyper crosslinked polymer, DOX delivery, biomacromolecules.

1. Introduction

In the evolving landscape of small molecule therapeutic use, there has been recent emphasis highlighting the importance of small molecules for chemotherapy in combination with several contemporary drug immunotherapy[1-3] and hormonal therapy[4-5] regimens for treating a wide array of cancers. On the grounds of this increased therapeutic use, overcoming the limited bioavailability of the small molecules has become the most important role of drug delivery systems since the majority of these drugs are insoluble in body fluids. The drug delivery system morphology and surface material enable improved control of the drug delivery. Predictable drug release kinetics can be optimized by altering the carrying capacity[6-8], limiting off-target toxicity[9], improving cellular uptake[10], and adjusting pharmacokinetics[11] adapted to the unique physiochemical properties of various small molecules. A major concern in the field of drug delivery systems is the biodegradability of these systems as they raise many environmental toxicology problems including various non-sustainable synthetic requirements, bioaccumulation, environmental persistence, and the unknown interactions of these molecules in water and air ecosystems[12-18]. Thus, new nanotechnologies rely primarily on biodegradable polymers in order to avoid environmentally harsh drug delivery systems[19-21]. These polymers can be synthesized by exploiting green engineering to fabricate innocuous renewable, biodegradable, biocompatible compounds. The usage of green engineering in concordance to the environmentally-friendly synthetic principles of green chemistry gave birth to the field of "green nanomedicine" with eco-friendly drug delivery systems with optimal drug loading and release[22]. Furthermore, there are various potent anticancer drugs from plant sources[23] and the incorporation of novel environmentally friendly drug delivery systems can potentially make the growing field of anticancer small molecules fully eco-friendly.

Nanocellulose fibers have been promising candidates among the polymers used for developing environmentally-friendly drug delivery systems[24]. The desirable drug delivery properties of nanocellulose including high availability of surface area, mechanical reinforcement, adjustable size and versatile surface functionalization are crucial for nano-scale bioavailability. These properties for enhanced anticancer drugs have been increasingly utilized, but are found to be limited with much room to grow[25]. Cellulose nanocrystals (CNC) are stable colloidal dispersions that are rod-shaped and are extracted from nanocellulose fibers. Nanorod formulations have more desirable drug delivery properties compared to nanospheres including tumor accumulation[26], prolonged half-life due to lower uptake by macrophages[27], and tumor homing due to unique rheology[28]. Hence, cellulose-based nanorod formulations have been advantageously used for drug delivery[29]. In order to resolve the low capacity of surface functionalization of CNC, hairy nanocelluloses (HNCs) have been produced by periodate oxidation which solubilizes the amorphous regions, and, at the same time, allows for the cleavage of cellulose chains in the crystalline regions leaving the soluble amorphous regions attached on both ends[30-31]. HNCs have dialdehyde-modified cellulose chains on both sides of the crystalline region and by oxidizing some of the aldehyde groups on the amorphous regions of HNC, bifunctional hairy nanocelluloses (BHNCs) can be synthesized, containing both aldehyde and carboxylic groups, further increasing the functionalization capacity of these nanocelluloses[32]. These cellulose derivatives are optimal guest polymers for the threading of Beta-Cyclodextrins (βCDs) supramolecular inclusion complexes and they have attracted great attention in recent years for developing advanced supramolecular materials with outstanding self-assembly and structural stability[33-34]. βCDs are cyclic oligosaccharides that consist of 7 glucopyranose units that form hydrophobic cavities and externally hydrophilic surfaces. The use of βCD nanoparticles for drug delivery has been extensive in research as they have shown to increase the bioavailability of many guests primarily due to the advantage of

using the well-known guest-host chemistry of isolated CDs for unique complexation of different guests. The supramolecular inclusion complex hides the hydrophobic host functionality in the interior cavity while the external surface hydroxyl groups of CD remain exposed to the aqueous environment. Functionalizing the alcohol groups of βCDs with several molecules (including ethylene diamine (EDA)) is known to enhance their physiochemical properties and can enable their cross-linking[35]. The unique supramolecular inclusion complexes of cyclodextrins makes them the stepping stone for the development of βCD-based polymers that largely optimize drug delivery depending on the drug's physiochemical properties. For example, βCDs were functionalized on hydrogels[36-38] and nanosponge[38] polymers that change the morphology of βCD making them less soluble and easily extractable. βCD can be substituted onto various polymers and CD-CD linkers can crosslink the polymers enabling hyper crosslinked βCD-based polymers. This has been shown to be more beneficial than the use of linkers alone to crosslink polymers since the hyper crosslinked βCD-based polymers have a larger specific surface area with more framework nanoporosity[39], allow better adsorption due to the accessible binding sites on the template. Moreover, these βCD-based polymers are observed to be thermally stable[40]. βCD-based polymers can host hydrophobic compounds in their internal cavity as well as hydrophilic compounds in the interstitial pores formed by the cross-linkers and the external CD walls. Importantly, most βCD polymers have predictable release schedules due to the polyester being predictably biodegradable[41] which puts them at an advantage compared to nanoparticles. The release is usually relatively very slow since the polymer network functionalized around the βCD cavity hampers the diffusion of entrapped guest molecules, thus promoting slower release kinetics[42]. The biodegradability of βCD polymers makes them candidates for use in the remediation of micropolluted water environments and ultrafast water treatment[43-44]. Combining βCDs with nanocellulose is highly beneficial for drug delivery due to the observed synergy between the

two materials for excellent biocompatibility, low cytotoxicity, biodegradability, efficient polymerization, and versatile functionalization[33]. In the present work, we hypothesize that BHNC can provide a colloidally stabilized structure and a template with a high carrying capacity for βCD-DOX supramolecular inclusion complexes forming green polymers with controllable drug delivery. In summary, we have developed a new rapid and green route to synthesize water-soluble and water-insoluble nanosponges using biodegradable materials. Here, nanosponges are defined as large nanoporous structures which are compressible and can adsorb water (or another solvent). Bifunctional hairy nanocellulose and beta-cyclodextrin materials have been crosslinked to each other with amide bonds. The extent of βCD grafting on BHNC will determine the solubility of the polymer along with the drug loading and release profiles. In this system, hairy nanocellulose particles are considered to be the backbone, and the immobilized cyclodextrin cavities capture the DOX (molecules) via host guest inclusion complexation. Moreover, the extent of cross-linking can be used for varying the morphology of the hyper-crosslinked polymer altering the release profiles and the solubility of the delivery system. Herein, we report, to the best of our knowledge, the first study that aims to use BHNC-βCD-EDA polymers for drug delivery aiming to expand the applications of BHNC. The polymerization of βCD-EDA with BHNC is fully characterized. This study advances the understanding of BHNC-βCD enhanced release profiles and its solubilizing capacity.

2. Experimental section

2.1. Materials and methods

Milled softwood kraft pulp sheets (Domtar, Inc., Canada) were used as precursors to the synthesis of BHNC. Sodium (meta) periodate ($NaIO_4$), sodium chloride (NaCl), sodium chlorite ($NaClO_2$, 80%), hydrogen peroxide solution (H_2O_2, 30%), ethylene glycol for oxidizing softwood pulp and hydroxylamine hydrochloride, sodium hydroxide (NaOH), and hydrochloric acid (HCl, 36.5-38.0%)

solutions for measuring the aldehyde content were purchased from Sigma-Aldrich. Beta-cyclodextrin ($C_{42}H_{70}O_{35}$, 99.9% (ELSD)) were purchased from AK Scientific. 1,1′-Carbonyldiimidazole ($C_7H_6N_4O$, 99.9%), Ethylenediamine ($C_2H_4(NH_2)_2$, 99.9%) for the synthesis of βCD-EDA from βCD, and DMTMM ($C_{10}H_{17}ClN_4O_3$, 96%) as a carboxyl activator, were obtained from Sigma-Aldrich. Anhydrous dimethylformamide ($HCON(CH_3)_2$, 99.99%), anhydrous ethanol (C_2H_5OH, 99.5%), and anhydrous acetone ($(CH_3)_2CO$, 99.8%) as solvents were purchased from Thermo Fisher Scientific. All chemicals were used as received and deionized (DI) water (resistivity of ~10 MΩ cm at 25 °C) was used in all experiments. Doxorubicin hydrochloride ($C_{27}H_{29}NO_{11}$) and phosphate-buffered saline (PBS, pH 7.4) for drug delivery experiments were supplied by Sigma-Aldrich were used in all experiments except where specified otherwise. Fetal bovine serum and penicillin/streptomycin solutions were purchased from Wisent bioproducts. Calcein-AM and Hoechst 33242 were purchased from AAT Bioquest and TOCRIS Bioscience, respectively. The human breast cancer cell line MDA-MB-231 was purchased from ATCC.

2.2. Preparation of bifunctional hairy nanocellulose (BHNC)

For the synthesis of BHNC, 12 g of milled softwood pulp was oxidized in 700 mL of a solution containing 16 g of $NaIO_4$ and 46.8 g NaCl at room temperature for 42 h under continuous stirring. The reaction beaker was wrapped with aluminum foil to prevent the deactivation of periodate, according to the procedure of Heidari Nia *et al.* with applying little changes[32]. 10 mL of ethylene glycol was added to this mixture. Ethylene glycol was used to quench the excess amount of periodate in order to stop the oxidation reaction. The product of the oxidation reaction, which is called dialdehyde modified cellulose (DAMC), was thoroughly washed with water using vacuum filtration. The aldehyde content of DAMC was measured by the hydroxylamine hydrochloride titration method as described in section 2.5.2. To convert half of the aldehyde groups to carboxylic groups, 6 g of as-

prepared never-dried DAMC was stirred at room temperature for 24 h with 7.5 g of $NaClO_2$, 24 g of NaCl, and 2.5 g of H_2O_2 in 600 mL of water. During this reaction, the conditions of the reaction were monitored by observing the color of the solution, with changed from dark fluorescent yellow to light yellow. Dark fluorescent yellow signifies that 0.1 M NaOH needs to be added, light yellow fluorescence means that the reaction is proceeding under optimal conditions, and a white color indicates that the reaction is completed. The oxidized pulp solution was filtrated with centrifugation at 8000 rpm for 10 min to remove the trace amounts of non-fibrillated fibers. The BHNC particles appeared in the form of a white precipitate after adding isopropanol 1.5 times the weight of supernatant. The precipitate was collected and purified through dialysis against DI water in 8-10 kDa dialysis bags with daily water exchanges for 3 days. The resulting neutral BHNC suspension was further dispersed by an ultrasonic processor (Hielscher UP200H, Germany) for 1 min. The synthesis of BHNC, used as a co polymer in this study, is shown in Scheme 1.

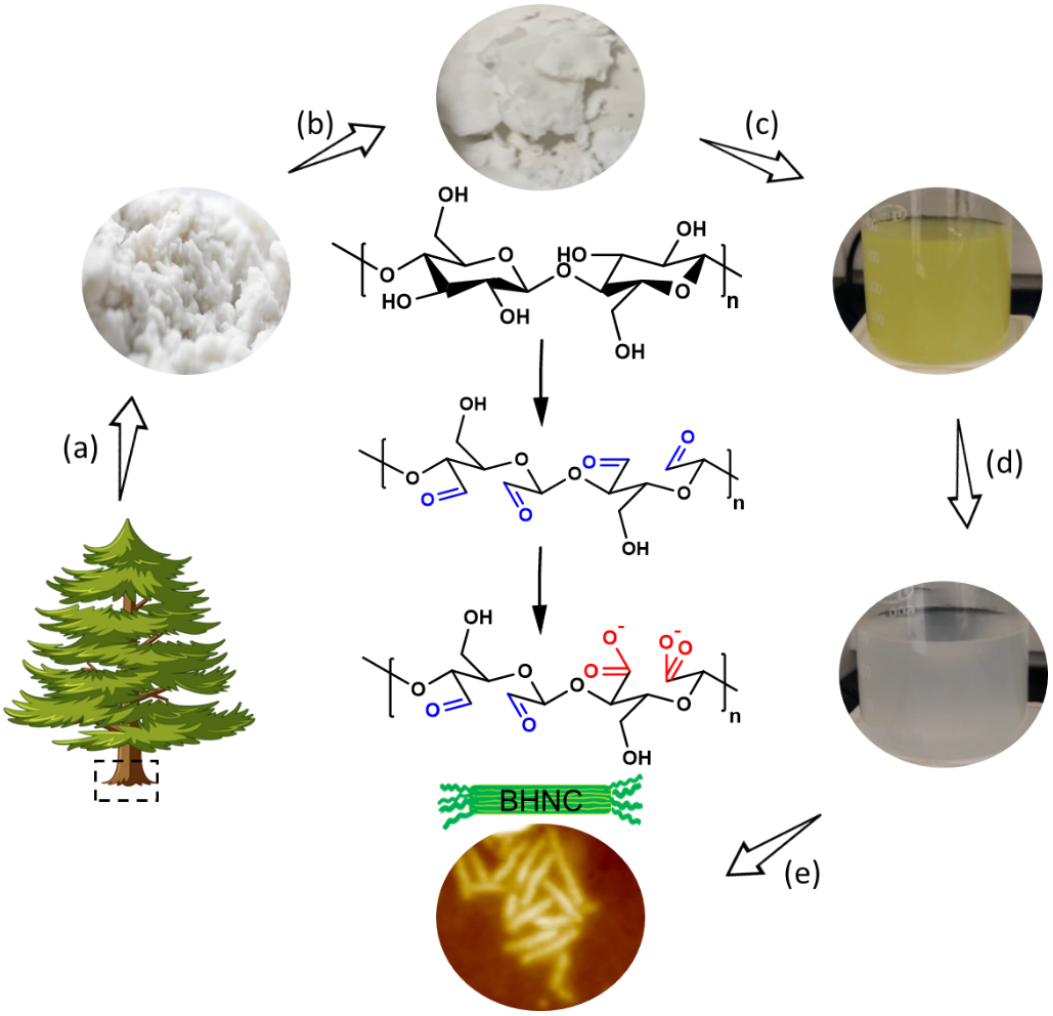

Scheme 1. Schematic illustration of the synthesis of the bifunctional hairy nanocellulose (BHNC) from cellulose nanofibrils by oxidation. a) Preparation of milled softwood pulp from wood, b) dialdehyde modified cellulose (DAMC) was prepared trough periodate oxidation, c) second oxidation process with sodium chlorite, d) monitoring the reaction by observing the color of the solution, with changing from dark fluorescent yellow to light yellow, and e) preparation of hairy nanocellulose after centrifugation and dialyzing.

2.3. Synthesis of hyper crosslinker βCD-EDA

βCD-CI. A simple nucleophilic substitution reaction method between 1,1′-carbonyldiimidazole (CDI) and hydroxyl groups on the surface of βCD, resulted in the formation of βCD-CI. Briefly 1.64 g of βCD and 1.96 g of CDI were dissolved in 30 ml DMF and then subjected to stirring with argon

protection at room temperature for 2 h. The white product obtained after the reaction was precipitated in cold diethyl ether and extracted with centrifugation. The resulting precipitate βCD-CI was washed several times with acetone. The white solid obtained by centrifugation was dried in a vacuum oven for 8 h to obtain a white powdery solid (1.43 g, yield: 87.2%).

βCD-EDA. Amine groups have been introduced on the surface of βCD through carbamate bonds between EDA and βCD-CI. In this synthesis, 1 g βCD-CI was dissolved in a high amount of EDA (40 mL) as a solvent in order to prevent the polymerization of βCD-EDA as EDA is the attacking material (nucleophile) of the carbonyl bond of βCD-CI. The solution was stirred at room temperature for 30 min under nitrogen protection, the final reaction mixture was heated to 40 °C under reflux conditions and held for 24 h with nitrogen protection. The resultant yellow precipitate was purified with the same method mentioned above and recrystallized with ethanol (0.92 g, yield: 92%). A schematic representation of synthesis of βCD-EDA and βCD-CI are shown in Scheme 2.

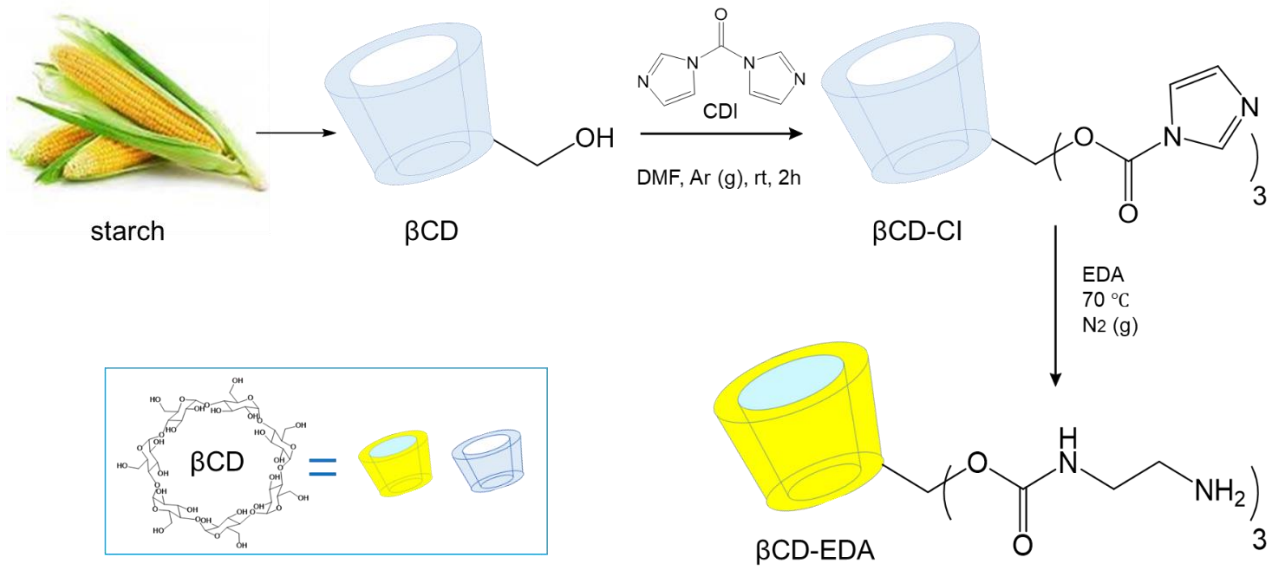

Scheme 2: Schematic illustration of the preparation of the hyper crosslinker βCD-EDA.

2.4. Preparation of water soluble and water insoluble polymerized hyper crosslinked BHNC-βCD-EDA (BBE)

Cellulose and βCD as bio-organic materials are good candidates for biocompatibility and sustainable drug delivery owing to the presence of a free amino groups per sugar unit in the hyper crosslinker βCD-EDA and free carboxyl groups in BHNC. So, the design of a natural polymerized hyper crosslinked BHNC-βCD-EDA (BBE) carrier is achieved through a facile crosslinking reaction with nucleophilic substitution of activated carboxyl groups of BHNC by amine arms of βCD-EDA (Scheme 3). βCD-EDA was wrapped around the BHNCs with amide bonds with different morphological shapes forming pH-responsive polymers. The hyper crosslinker βCD-EDA was polymerized with BHNC particles with the help of DMTMM as an activator reagent in water at low temperature. DMTMM is considered a green activator that can be extracted after the activation of the carboxylic content. Unlike other polymer-based βCDs and βCD-based nanosponges, these new types of crosslinked polymer were prepared in a green and safe solvent (water) and with very short reaction times and at low temperatures. The reaction was started by activating different ratios of the carboxyl content of BHNC with DMTMM (100% (1/1; activated carboxyl content to DMTMM), 50% (1/2), 25% (1/4) and 12.5% (1/8)). Briefly, different amounts of DMTMM (37.2, 18.6, 9.3 and 4.65 mg) were added to the 7.5 mL BHNC suspension (3.8 mg/mL with 4.5 mmol/g carboxyl content) and stirred for 5 min at 37 °C and then, the desired amount of βCD-EDA (164, 82, 40 and 20 mg) was dispersed in 20 mL water and added to the activated BHNC solutions. The resulting solutions were stirred for 1 h at 37 °C. After less than 5 minutes. For BBE1/1 and BBE1/2, a yellow solid was produced while for the other polymers (BBE1/4 and BBE1/8) the solution remained transparent yellow. Afterwards, all the solutions were purified through dialysis against DI water in 8-10 kDa dialysis bags with daily water exchanges for 3 days. The obtained solutions were lypholized and the βCD-EDA content was measured gravimetrically and with a phenolphthalein assay (see figure S1).

237

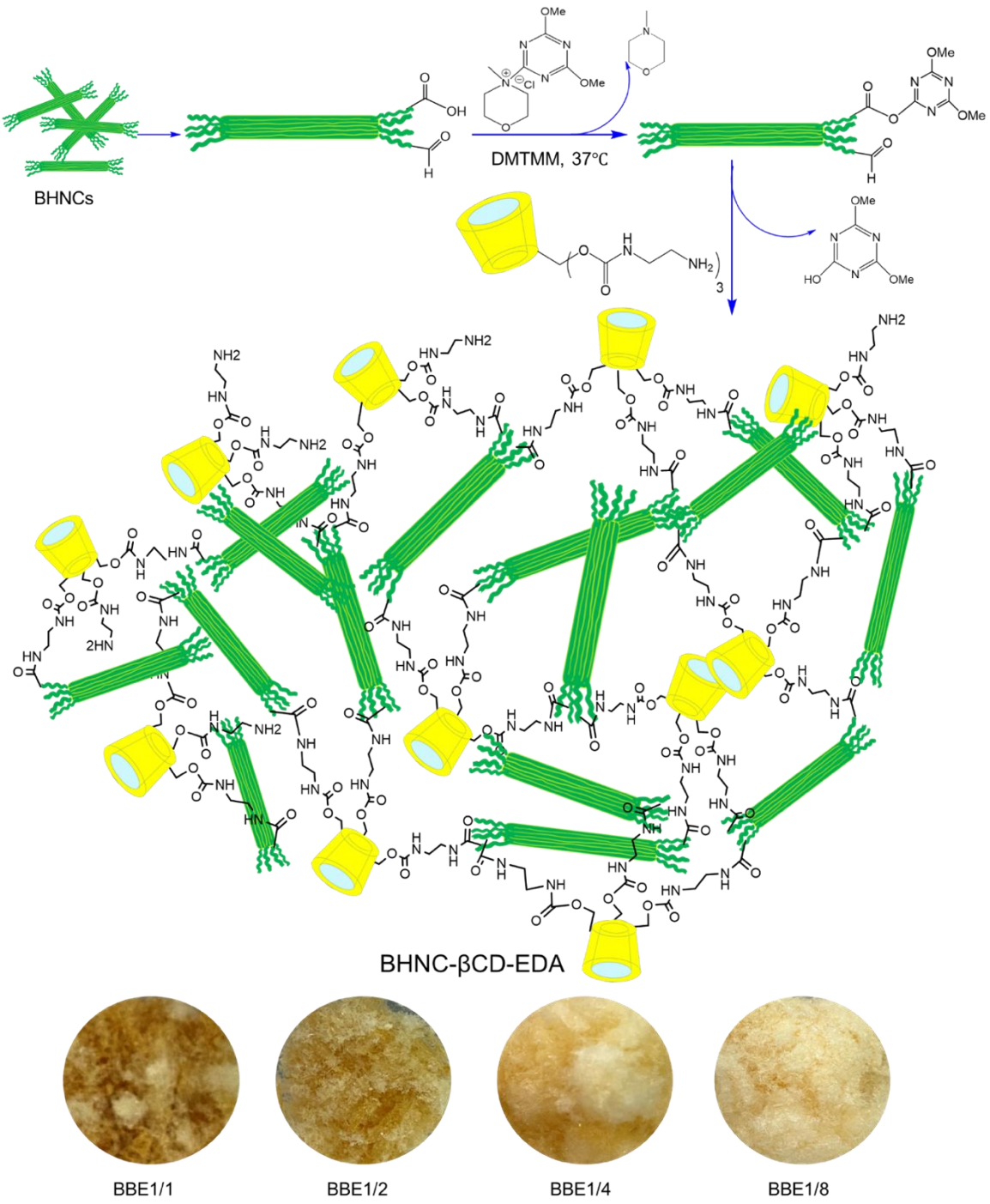

Scheme 3. Schematic illustration of one-pot synthesis of polymerized hyper crosslinked BHNC-βCD-EDA (BBE).

2.5.Characterization of BHNC, hyper crosslinker βCD-EDA, water soluble and water insoluble polymerized hyper crosslinked BHNC-βCD-EDA (BBE)

Morphological characterization

Transmission electron microscopy (TEM). The morphology and particle size of BHNC were investigated using TEM. The images were obtained with a Philips Tecnai 12, operating at 120 kV, equipped with a Gatan 792 Bioscan 1000 × 1000 wide angle multiscan charge-coupled device (CCD) camera. The TEM specimen were prepared from a suspension of the samples with a concentration of 0.1 % (w/w) in the corresponding particular solvent. A drop of the suspension was placed on a copper grid coated by a thin carbon film and the drop was left to evaporate.

Field emission scanning electron microscope (FE-SEM) The morphology of the βCD-EDA and BBE hyper crosslinked polymers were characterized using FE-SEM. The samples were prepared by dropping the solution onto a coverslip, followed by evaporating the liquid in air and coating with a 3 nm thick layer of Pt by a high-vacuum coater (Leica EM ACE600). FE-SEM images were recorded on a Q450 ESEM (FEI quanta 450 environmental scanning electron microscope). The images were taken at an accelerating voltage of 7 kV.

Atomic force microscopy (AFM). The surface morphology and size of BHNC nanoparticles were recorded by AFM with Nanoscope IIIa controller (Digital Instrument/Veeco, Santa Barbara, CA). To prepare the AFM sample, a freshly cleaved mica was inclined to a magnetic disc by double-sided tape and coated with 0.1% poly-l-lysine (PLL). After 5 min, the excess PLL was rinsed off with Milli-Q water. A drop of BHNC suspension with concentration of 0.1 mg/mL was placed on a freshly cleaved mica surface for 10 min, followed by washing off the excess liquid with Milli-Q water. Before measurement, samples were air-dried overnight. The experiments were conducted in tapping

mode with a silicon probe (Nanoworld; type: SSS-NCH) with force constant of 42 N/m, resonance frequency ~320 kHz, and nominal tip radius ~5 nm.

Aldehyde content of DAMC and BHNC

The aldehyde content of DAMC and BHNC was determined using the hydroxylamine-hydrochloride titration method that was introduced in our previous work[32]. Shortly, the exact amount of oxidized sample was suspended in water and the pH was adjusted to 3.5 using HCl. Afterwards, the pH of the 10 mL hydroxylamine-hydrochloride solution (5% w/w) was adjusted to 3.5 using NAOH solution which was added to the sample suspension under vigorous stirring until the oxime and HCl form and consequently, the pH drop was observed. The resulting HCl was titrated with NaOH solution (0.1 M) until the pH becomes constant at 3.5. The aldehyde content was calculated using the following formula:

$$\text{Aldehyde content (mmol g}^{-1}) = V_{NaOH} \times N_{NaOH} / W_{(DAMC \text{ or } BHNC)}$$

where V_{NaOH} is the volume of titrant (mL), N_{NaOH} is the normality of titrant (mol L^{-1}), and W is the weight of dry samples (g) initially suspended.

Carboxylic content of BHNC and amide content of βCD-CI

The carboxylic content of BHNC and the amide content of βCD-CI were measured with conductometric titration. Briefly, 5 mL of BHNC solution (2 mg/mL) or a certain amount of βCD-CI were added to a 100 mL milli-Q water and 1 mL NaCl solution (20 mM). The pH of the solution was adjusted to 3.5 by adding HCl (0.1 M) and the mixture was moderately stirred. Thereafter, using titrando titrator (Metrohm836, Switzerland), 10 mM NaOH solution were added to the solution with a rate of 0.1 mL/min until the pH reached to around 11 (see figure S2 and S3). The carboxylic content was determined from the following equation:

Carboxylic content (mmol g^{-1}) = $V_{NaOH} \times N_{NaOH} / W_i$

where V_{NaOH} is the volume of titrant (mL), N_{NaOH} is the normality of the titrant (mol L^{-1}), and W_i is W_{BHNC} or $W_{\beta CD\text{-}CI}$, being the weight of BHNC or βCD-CI used initially (g).

Phenolphthalein (PHTH) assay for βCD grafting ratio of BBEs

In order to measure the amount of active βCD grafted on BHNC, phenolphthalein was used as a quantitative alkaline calorimetric indicator that could insert into the active βCD cavities. Briefly, increasing amounts of βCD were added to the PHTH solution containing 0.02M $NaCO_3$ buffer at pH 10.5 with freshly prepared 0.5×10^{-3} g.mL^{-1} PHTH and the absorbance was measured by UV–Vis spectrophotometry at 550 nm corresponding to the deprotonated PHTH in the βCD cavity. Thereafter, a standard curve was plotted as absorbance vs βCD concentration in g/L (see Figure S1a). 10 mg of each of the BBE polymers was added to 25 mL of the phenolphthalein solution, stirred, and equilibrated overnight and the absorbance was measured and the βCD concentration in the polymers was determined by referring to the standard curve. PHTH does not bind to the BHNC pristine and the measured absorbance would hence only reflect PHTH in the βCD cavities[45]. The βCD content of the BBE polymers was determined using the following equation:

$$\beta\text{CD } content \text{ (mmol } g^{-1}) = \frac{V C_{\beta CD}}{m M_{\beta CD}}$$

Here V is the volume of the solutions (mL), $C_{\beta CD}$ is the concentration of βCD obtained from the calibration curve (g L^{-1}), m is the mass of the BBE samples (g), and $M_{\beta CD}$ is the molar mass of βCD (g mol^{-1}).

Amine content of βCD-EDA

The amine content of βCD-EDA was measured using a titration. Firstly, 5 mg BHNC were dissolved in 100 mL milli-Q water. The pH of the solution was adjusted to 9.5 by adding NaOH (0.1 M) under vigorous stirring. Thereafter, using a titrando titrator (Metrohm836, Switzerland), 10 mM HCl solution was added at a rate of 0.1 mL/min until the pH reached about 3.5 (see figure S4). The amine content of βCD-EDA was calculated by the following equation:

$$\text{Amine content (mmol g}^{-1}) = V_{HCl} \times N_{HCl} / W_{\beta CD\text{-}EDA}$$

where V_{HCl} is the volume of titrant base (mL), N_{HCl} is the normality of the titrant base (mol L^{-1}), and $W_{\beta CD\text{-}EDA}$ is the weight of βCD-EDA that used initially (g).

Particle size measurements using dynamic light scattering (DLS) and Zeta-potential analysis by electrophoretic light scattering (ELS)

The equivalent spherical hydrodynamic diameter and polydispersity of the BHNC and BBE samples were determined by a Brookhaven light scattering instrument (BI9000 AT digital correlator). In all DLS experiments, the scattered light intensity was measured at a 90° scattering angle and at 25 °C. For preparing the samples, 100 µL of 0.1% (w/w) BHNC suspensions and BBE samples were added to 900 µL of DI water in low-volume disposable cuvettes. The magnitude of the surface charges of the particles was monitored using a Zetasizer Nano ZS (Malvern instrument, Lt.d., U.K.). To measure the zeta potential data, the suspensions of BHNC and BBEs were diluted to 0.1% (w/w) with DI water.

Fourier transform infrared (FTIR) spectroscopy

Functional groups in the structure network of BHNC and BBEs were identified using a FTIR spectrometer (PerkinElmer, Inc., Waltham, MA, U.S.A.) equipped with a single bounce diamond attenuated total reflectance (ATR) cell. The completely dried samples were placed directly on the

ATR crystal. All FTIR spectra were averaged from 32 scans from wavelengths 400 to 4000 cm^{-1} with a resolution of 4 cm^{-1}.

Surface area and pore size analysis

N_2-sorption was measured on a Tristar 3000 from Micromeritics, and the data for the BET plot fitting, specific surface area and pore size distribution of the particles were analyzed by Tristar 3000 software package V6.07. Since the results are expressed in units of surface area per gram of sample, the true sample mass must be known and hence, solid samples were meticulously weighted (0.1 g <weight <1 g), degassed at 120 ºC and purged with N_2 for 24 h. The pore size distributions of the different BBE bio-polymers were calculated using the Barrett–Joyner–Hollande (BJH) model based on the adsorption and desorption branches of the isotherms.

Thermal gravimetric analysis (TGA)

The thermal stability of BHNC, βCD, and BBEs was investigated with a thermal gravimetric analyzer (Discovery 5500, TA Instruments, USA). To prepare the samples for analysis, around 5-10 mg were placed on a little trace and automatically reweighted with TRIOS instrument. Heating temperature was chosen between 20 to 1200 °C with a controlled heating rate of 0.1-1500 °C min^{-1} in a controlled atmosphere. The flow rate of high purity N_2 gas was 50 mL min^{-1}.

Powder X-ray diffraction (PXRD)

The presence of the BHNC crystalline region after polymerization with βCD-EDA with examined with XRD. The measurements were performed on a Bruker Discover D8 Discover two-dimensional diffractometer with VANTEC 2D detector and CuKα radiation (λ=1.54 Å). The X-ray diffractograms were acquired at 40 kV and 40 mA with a 2Θ (Bragg angle) range of 10-30º at a scan rate of 0.005º s^{-1}.

Solid-State carbon-13 NMR

Solid carbon-13 NMR data was acquired using a VNMRS 400 widebore spectrometer operating at 399.9 MHz for ^{1}H and 100.5 MHz for ^{13}C in a 4 mm Varian Chemagnetics double-resonance probe. The recycle delay was 4 s. The sample was spun at 8 kHz. The CP contact time was 2 ms, and a total of 12000 scans (17 hours) were collected.

Liquid-State hydrogen and carbon-13 NMR

The 13C NMR spectrum (126 MHz, D2O) was acquired using a Bruker AVIIIHD spectrometer using a BBFO and Smart Probe. The ^{1}H spectra (500 MHz, D2O) were acquired using a Varian VNMRS using a switchable broadband probe. 3000 scans were used for the ^{13}C spectrum and 16 for the proton,

2.6. Preparation and characterization of DOX-loaded BBEs

DOX loading

DOX loading of BHNC and BBEs was carried out by dispersing 10 mg samples in 1 mL ultrapure water and 500 μL DOX solution (10 g/mL). The final mixtures were kept in a dark area and incubated on a magnetic stirrer at 800 rpm overnight. Then, samples were collected using ultra-centrifugation (12000 rpm, 10 min) and after several washes, the supernatants were used to determine the DOX-loading efficiency into the particles by UV–vis spectrophotometry at 480 nm. A calibration curve specific to DOX was prepared to convert the absorbance to DOX concentration. The amount of DOX loaded into the samples was calculated using the following equation (2):

$$q_e(\text{mg DOX/g samples}) = \frac{(C_0 - C_e)\text{V}}{m} \qquad (2)$$

where C_0 is the initial concentration of DOX (mg/L), C_e is the concentration of DOX at equilibrium (mg/L), V is the volume of DOX (L), and m is the mass of samples (g). The equilibrium DOX uptake (q_e) is expressed in mg DOX per g samples.

Release profile

In vitro release of DOX from the BHNC-DOX and BBEs-DOX was measured by UV-Vis. Briefly, a series of BHNC-DOX and BBEs-DOX were respectively dispersed in 1 mL of PBS (pH 5.5, 6.5 and 7.6) and vigorously stirred for 160 h at 120 rpm at 37 ℃. After specified time periods, 1 mL release solution was taken out and replaced with an equal volume of fresh fluid. The release of DOX from PBS solution was monitored at 480 nm by UV–Vis. The procedure of drug loading and release is shown schematically in Scheme 5.

Scheme 5: Schematic illustration of DOX loading in pH-responsive BBE structures and BHNC as a control structure.

Biocompatibility tests

The toxicity of BBE and DOX loaded BBE was tested with MDA-MB-231 breast cancer cell lines. MDA-MB-231 was cultured in DMEM medium with 10% fetal bovine serum, 100 U/mL penicillin, and 100 μg/mL streptomycin at 37 °C and 5% CO_2 until 80% cellular confluency was attained. Cells

were harvested and 6,000 cells/well were seeded into a 96-well plate and cultured for 24 h. The medium was then replaced by a fresh medium containing BBE-DOX prepared from ultrapure water, containing a 10 mg/mL BBE1/4-DOX stock solution loaded with 835 µM doxorubicin and 15 mg/mL or BBE1/1-DOX containing 732 µM loaded-doxorubicin. Our previous experiments show that 5.04 µM DOX has a more remarkable toxic effect on MDA-MB-231 cells when exposed for 24 h[29]. A final concentration of 5.04 µM BBE-DOX was used (based on BBE-DOX loading), and incubated at 37 °C and 5% of CO_2 for 24 h. As controls, we used MDA-MB-231 culture without BBE structures, (BBE-Free (without doxorubicin), 10 mg/mL or 15 mg/mL stock solution for BBE1/4 and BBE1/1, respectively), and doxorubicin (Dox, at 5.04 µM). Calcein-AM and Hoechst 33242 were used to measure cell viability and nuclear staining, respectively. After incubation, the culture medium was removed and the wells were washed three times with DPBS (Dulbecco's phosphate-buffered saline). For viability, 100 µL working solution composed of 1 µL of Calcein-AM (4 mM) and 2 µL of Hoechst (18 mM) in 1 mL of DPBS was added per well and incubated for 45 min at 37 °C. Spinning-disk confocal microscope Olympus IX83 was used to obtain the confocal microscopy images. By manual counting the viability was determined using the following equation (3):

$$\%\ of\ viability = \frac{\#\ live\ cells}{\#\ total\ cells} \times 100 \qquad (3)$$

Ethidium homodimer I or propidium iodide were not used as dead cell markers since doxorubicin interferes with the measurement. All experiments were performed in quadruplicates.

3. Results and discussion

3.1.Characterization of BHNC and bio-derived BHNC-βCD-EDA trifunctional polymerized nanosponges (BBEs)

Morphological, structural and dimensional analysis

The morphologies and the dimensions of rod-like BHNC particles and the different structural morphologies of polymer-based BBEs in three different conditions (freeze-dried, non-freeze dried and supramolecular inclusion complex with DOX) were evaluated with AFM, TEM, HRTEM and FE-SEM imaging. BHNC nanorods were analyzed using both AFM (Figure 1a), TEM (Figure 1b) and HRTEM (Figure 1c). TEM and HRTEM images of BHNC clearly show the typical rod-like nanoparticles with a more or less uniform size and shape (Figure 1b and 1c). The BHNC polymer template particles have, on average, a length of about 150 nm and width of about 5 nm. AFM images of the BHNC particles shown in (Figure 1a) reconfirm the morphology and dimension properties of BHNCs. DLS showed an average size of BHNC particles of 138 nm with a polydispersity of 0.21 (Table 1).

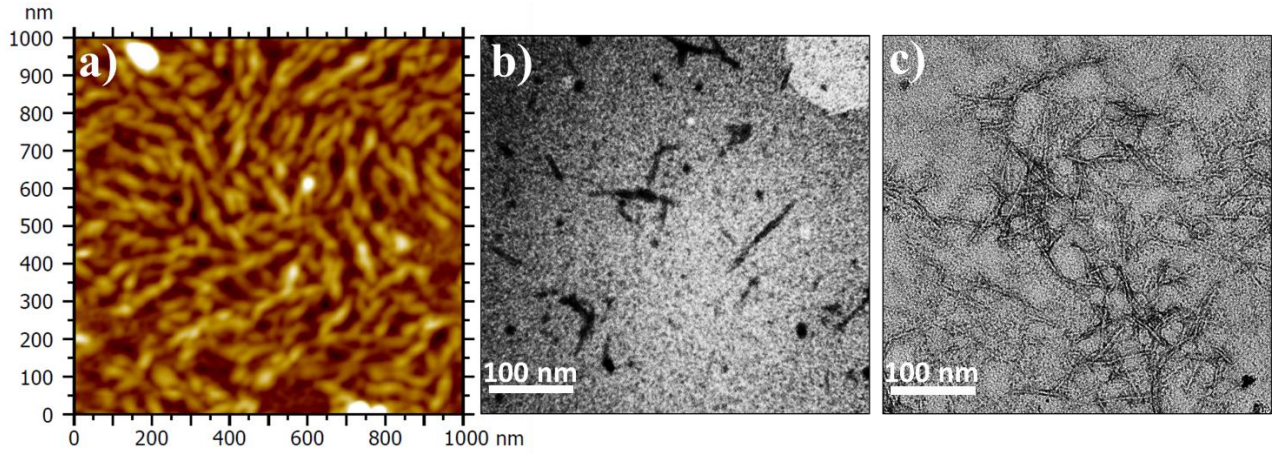

Figure 1: (a) AFM, (b) TEM, and (c) HRTEM images of BHNC rod-shape particles used as building blocks for preparation of polymer-based BBEs.

Biopolymer-based BBEs with different physical properties at two different conditions (freeze-dried and non-freeze dried) were analyzed by FE-SEM (Figure 2a-i) and (Figure S5-7). These images demonstrate that each of the 4 synthesized BBEs has a different structure before and after drying. The SEM images of β-cyclodextrin (Figure S5) revealed that the material displayed a dense block-shaped morphology with uniform shapes and flat surfaces. After functionalization with EDA, the white βCD turned yellow, which indicated that the crosslinking reaction had successfully occurred. Besides, as shown in (Figure 2a), unlike the pristine βCD, the surface of the modified βCD, (βCD-EDA), became extremely loose and uneven, and displayed an evidently porous structure. Hence, it is clear that the pristine βCD-EDA has an amorphous morphology and this morphological irregularity was diminished by functionalization with the rod-like BHNC as seen from the uniformly ordered morphologies in the different BBE SEM images. After polymerization of BHNC with βCD-EDA, it is obvious that the BBEs presented a different morphology compared to BHNCs. For better understanding, the different morphologies of BBEs with different βCD-EDA contents are presented in Figure 2. FE-SEM images in Figure 2b and 2c are those of BBE1/1 with the highest amount of βCD-EDA and both non-freeze dried and dry samples of BBE1/1 consist of water-insoluble nanosponges. Both images exhibit a spongy structure that makes the bio-polymers absorptive for DOX. Surprisingly, the morphologies of BBE1/2, 1/4 and 1/8 were completely different from BBE1/1 and furthermore, each of these 4 types of BBE biopolymers had different morphologies in the non-freeze dried and dry state. In BBE1/1 and BBE1/2 with increasing amounts of βCD-EDA, different extents of agglutination between BHNC and βCD-EDA resulted in water-insoluble nanosponges with different structures. As can be seen in Figure 2d and 2e, BBE1/2 nanosponges have totally different structures: in non-freeze dried conditions BBE1/2 has the expected rod-shape polymerized fibrous architectural structure that is due to the BHNC particle morphology, and the freeze-dried structure

consists of microspheres with an average size of 2-6 µm. It is observed that with decreasing βCD-EDA content in the polymerization process, the presence of BHNC finger-print as a building template in the polymerized product is more obvious, especially for the BBE1/4 and BBE1/8. Unlike the non-freeze dried condition, after freeze-drying the samples, BBE1/4 and BBE1/8 nanosponges had decorated rod-like morphologies with an average thickness of 4-6 µm and they possesses micro-rod sites and some micro-sheets (Figure 2f and 2h). An important morphological property observed in the FE-SEM images of non-freeze dried BBE1/4 in Figure 2g is the unique agglutination between BCD and BHNCs which resulted in remarkable helical morphologies. These helical structures are less than 200 nm in diameter and have a left-handed twist. Cellulose nanocrystals are known to form chiral nematic phases with helical nanorod arrangements; they also form in the presence of polymer. The FE-SEM image of these unique helical structures is shown enlarged in Figure 3 (left). A possible explanation of how these structures are formed is shown in Figure 3 (right). They could be formed by crosslinking the hairs of the BHNC nanorods by βCD-EDA, with subsequent near alignment of the cellulose nanocrystals. Moreover, FE-SEM images of non-freeze dried BBE1/8 (with the lowest amount of βCD-EDA) clearly show that this type of nanosponge has a fibrous structure with very thin fibers (Figure 2i), which might have a similar structure as fibrils from BBE1/4. In summary, the FE-SEM images of BBE1/2, BBE1/4, and BBE1/8 (Figure 2e, 2g, and 2i) show that BHNC nanorods are trapped and polymerized with βCD-EDA in different morphologies. Hence, the polymer network morphology is strongly dependent on βCD-EDA monomer content.

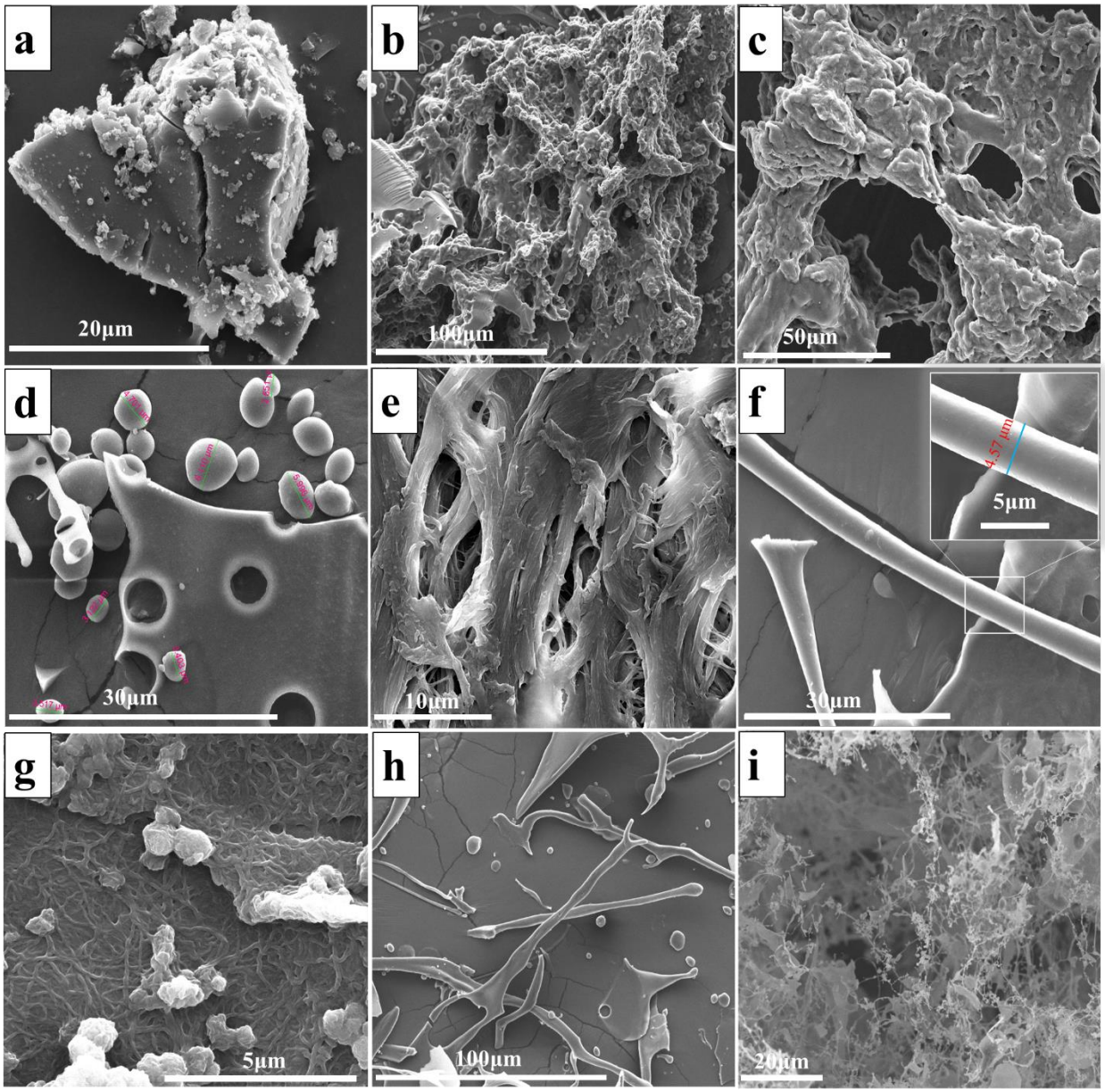

Figure 2: FE-SEM images of; (a) pristine βCD-EDA; (b, c) freeze dried and non-freeze dried BBE1/1 nanosponge; (d, e) freeze dried and non-freeze dried BBE1/2 nanosponges, (f, g) freeze dried and non-freeze dried BBE1/4; and (h, i) freeze dried and non-freeze dried BBE1/8 with different magnifications.

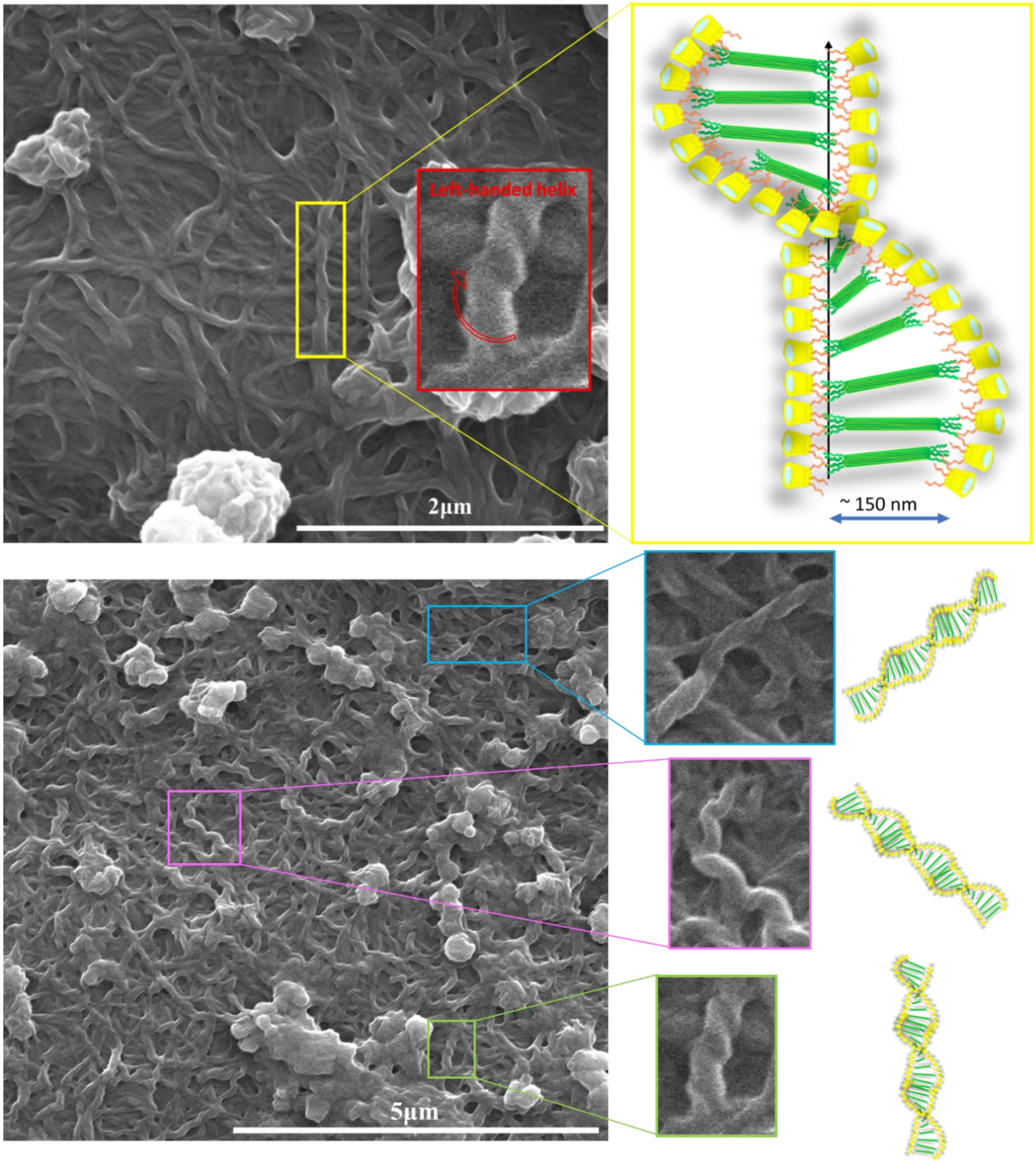

Fgure 3: (Left): FE-SEM image showing left-handed helical BBE1/4 fibrils; (Right): possible structure of helical fibrils, formed by hairy nanocellulose rods (green with hairs), crosslinked at their ends by βCD-EDA (yellow with red carbamate-EDA arms).

Further morphological investigation of different BBE biopolymers in physical mixtures with DOX unveiled an outstanding morphology for these nanosponges and the supramolecular inclusion complex of DOX-BBEs were observed under FE-SEM images (Figure 4a-i). As expected, the pristine structure of DOX with clear columnar crystal edges and corners morphology are shown in (Figure 4a). The FE-SEM images represent the cubic crystalline sites of DOX in all of the mechanical mixing structures with BBEs marked with red circles (Figure 4b, 4d, 4f and 4h), and in all of these images, BBE morphologies remained unchanged (marked with yellow squares). The supramolecular inclusion complexes in the non-freeze dried nanosponges can be seen in Figure 4c, 4e, 4g and 4i, where they appear with different polymerized architectural morphologies. When compared, the morphology of the non-freeze dried BBEs and their supramolecular inclusion complex structures are very similar. Clearly, there is strong evidence of the presence of BHNC particles in the supramolecular inclusion complexes. Also, the helical polymerizable liquid crystal-like assemblies of BHNC particles were also seen in FE-SEM images of supramolecular inclusion complexes of BBE1/4 with DOX (Figure 4g). In breast cancer cells, helical DOX-BBE1/4 showed the minimal cell viability compared to the control or DOX cultures, suggesting that DOX-BBE1/4 has a greater anticancer effect than free DOX. Compared to BBE1/1 (with higher DOX capacity), the effect on the breast cancer was approximately the same.

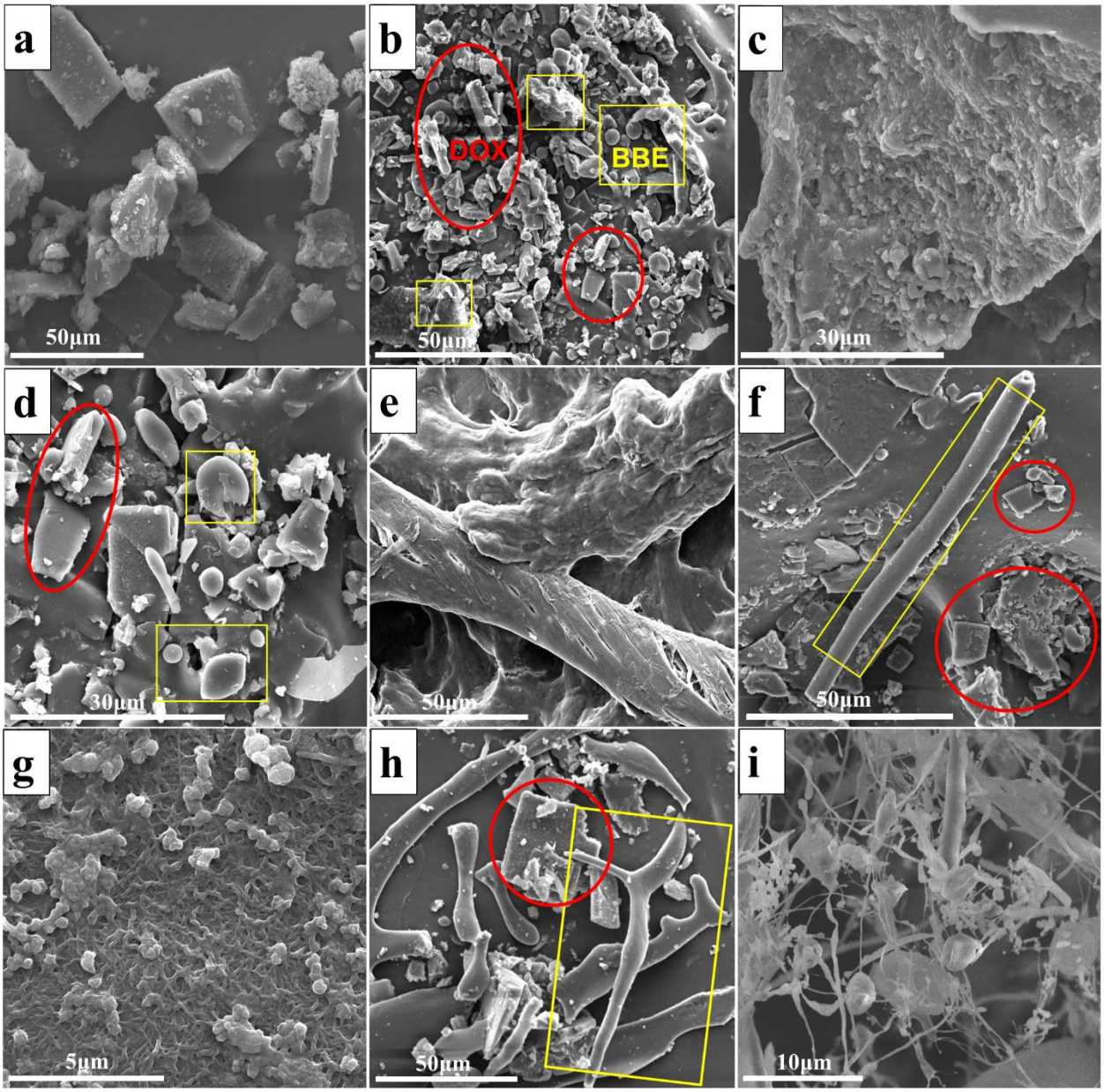

Figure 4: FE-SEM images of; (a) DOX cubic crystalline particles; (b, c) physical mixture and supramolecular inclusion complex of DOX with BBE1/1 nanosponges. In red circles: DOX cube-shape morphology. In yellow boxes: BBE loaded DOX with different morphologies are shown; (d, e) physical mixture and supramolecular inclusion complex of DOX with BBE1/2 nanosponges; (f, g) physical mixture and supramolecular inclusion complex of DOX with BBE1/4 nanosponges; and (h, i) physical mixture and supramolecular inclusion complex of DOX with BBE1/8 nanosponges.

FTIR spectroscopy

To confirm the structure of BHNC particles as building blocks in polymerized products obtained from soft wood pulp and DAMC and to confirm the surface modification of the precursor, FTIR spectra of the different nanocelluloses, βCD, βCD-CI, and βCD-EDA were collected (Figure 5a-d). The results displayed in Figure 5a suggest that along with the characteristic cellulose peaks at 3310 cm^{-1} (stretching vibration modes of −OH groups), 1306 cm^{-1} peak (−OH bending vibration), 2909 cm^{-1} peak (C–H stretching vibration), 1426 cm^{-1} peak (−CH_2 scissoring), 1034 cm^{-1} peak (CH_2–O–CH_2 stretching), and a very small peak at 1630 cm^{-1} (cellulose carboxyl vibration in the sodium form), wet DAMC had two characteristic peaks at 1730 cm^{-1} related to non-protected aldehydes and 880 cm^{-1} related to the dialdehyde group hemiacetal linkages. Compared to the FTIR spectrum of DAMC, the BHNC spectrum had a sharp increase in the 1603 cm^{-1} peak related to carboxyl vibration in the sodium form, indicative of successful oxidation of surface aldehyde groups to carboxylic acid. However, the oxidation was not complete since the aldehyde peaks persist in the BHNC spectrum with the 880 cm^{-1} peak (unprotected dialdehyde group hemiacetal linkages in BHNC particles) and the 1730 cm^{-1} protected aldehyde group peak which is expected to overlap with the strong carboxylic acid 1603 cm^{-1} peak. That βCD functionalization with EDA for preparing the EDA arms on the βCD body had occurred, was confirmed by FTIR, as can be concluded from Figure 5b. Firstly, the nucleophilic hydroxyl groups located on the C_6 of βCD attacks the carbonyl of CDI and one of the imidazoles that acts as a leaving group is replaced with the nucleophile. As a result, new unique carbonyl peaks for carbamate bonds were observed in the FTIR spectrum of βCD-EDA at 1741 cm^{-1}. On the other hand, as can be seen in Figure 5b, comparing βCD-CI to CDI shows that the unique hydroxyl groups attributed to βCD at 1010 cm^{-1} and the aromatic amine peaks for imidazole in CDI at 1267 cm^{-1} are only present together in the βCD-CI spectrum. Furthermore, the imine stretching peak at 1640 cm^{-1} is observed in βCD-CI and CDI confirming successful functionalization of

carbonyl-imidazole on βCD. This suggests that the resonance electrons are only shared between the carbonyl and imidazole in βCD-CI confirming the site of the nucleophile attack to be the carbonyl of CDI. Secondly, the EDA nucleophilic attack on the carbonyl of βCD-CI is confirmed with the introduction of the new EDA band at 1637 cm^{-1} corresponding to N-H bending vibration. The successful preparation of bio-derived BHNC-βCD-EDA trifunctional polymerized nanosponges was observed with FTIR in Figure 5c. The successful novel bio-polymeration of the BBE nanosponges can be confirmed through the amide bond formation between the activated carboxyl content in BHNC and the primary amines of βCD-EDA. This characteristic peak overlaps with two other broad characteristic double peaks at 1722 cm^{-1} and 1736 cm^{-1} attributed to the carbonyl vibration of aldehydes on the BHNC and carbonyl vibration band of carbamate related to βCD-EDA respectively. The disappearance of the peaks at 1603 cm^{-1} that corresponds to carboxyl stretching vibrations on the BHNC is good evidence for proving that the polymerization of βCD-EDA with BHNC building blocks has occurred. Finally, to verify that there are no differences between different types of bio-derived BHNC-βCD-EDA trifunctional polymerized nanosponges, the FTIR spectra were compared in Figure 5d. It is evident that the trifunctional polymerization fabrication of BHNC particles with βCD-EDA via a facile and green one-pot crosslinking reaction method using EDA as a cross-linker (BHNC-βCD-EDA). There are no structural changes observed between them. The only difference was for the EBB1/8 structure that had a sharper carboxyl vibration band at 1603 cm^{-1} which confirms that the BBE1/8 has the highest carboxyl content compared to the other BBE polymers.

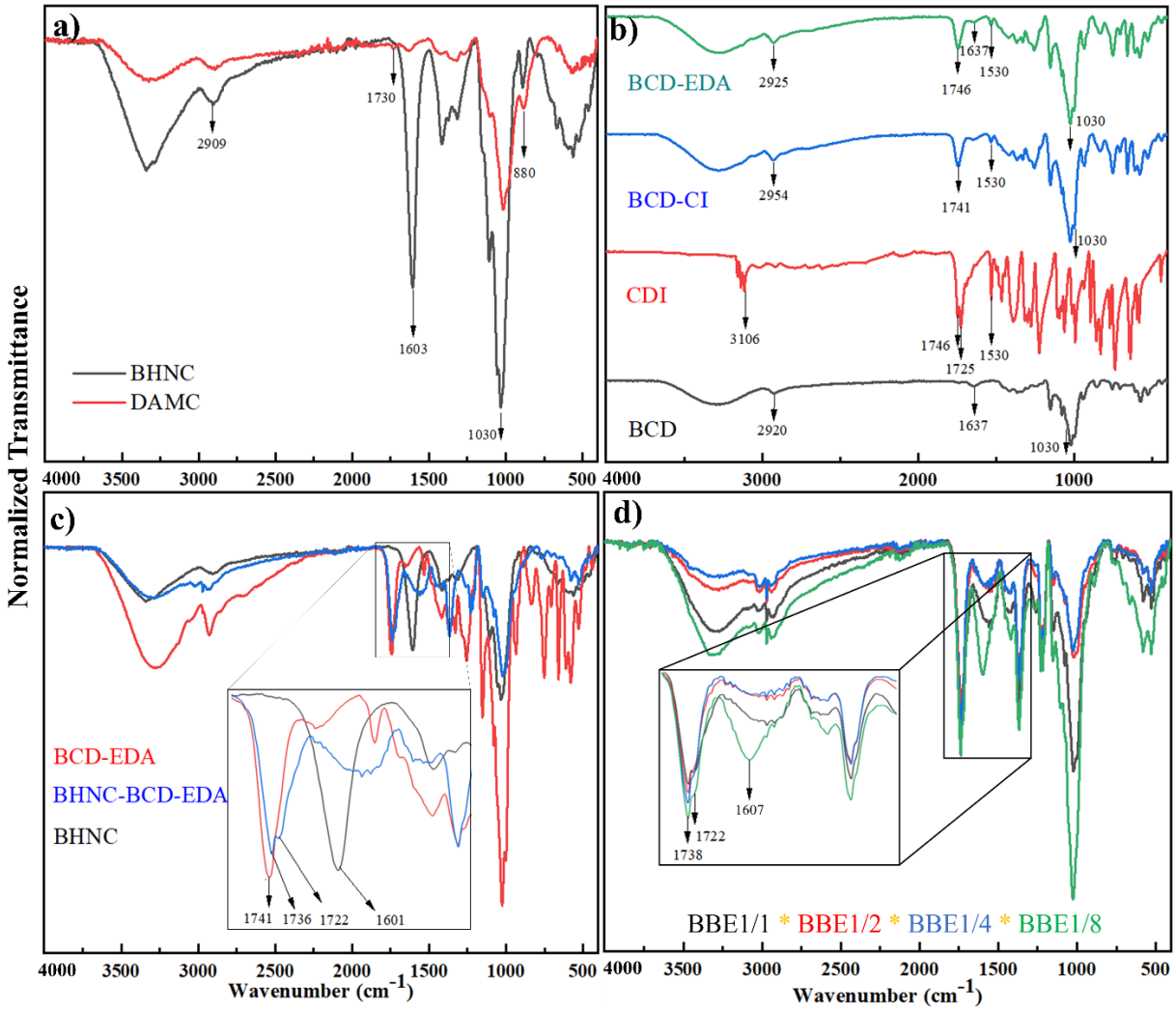

Figure 5: FTIR analysis of different control materials in each preparation steps and trifunctional BBE biopolymers.

XRD

The crystallinity of the BBEs was investigated by XRD (Figure S8). The results indicated that the high index of crystallinity of BBE corresponds mainly to BHNCs which are crosslinked with βCD and shows a peak around 20.5◦, characteristic for cellulose crystals with Miller index (021).

TGA

The TGA curves of BHNC and trifunctional BBE biopolymers are shown in Figure 6. The thermal behavior of the biopolymers involves only a three-step process with two isothermal conditioning periods. At the first step all samples showed a decrease in weight below 150 °C owing to the evaporation of physically absorbed water on the surface of biopolymers (10%). The second and third steps account for most of the weight and results in the formation of the residue of the βCD polymer and cellulose. For dried bifunctional hairy nanocellulose, the disintegration at the second stage (the first pyrolysis stage) occurs at 200-300 ºC and was mainly caused by the degradation of cellulose chains, showing a drastic weight loss of 45%. The third stage (second pyrolysis stage) at 300-600 ºC was caused by the slow carbonization of cellulose and was accompanied by a 20 % additional weight loss. For BBE, the second degradation stage of biopolymers takes place at a higher temperature (200-350 °C) than for BHNC, with high weight loss (50%), and the third degradation stage of biopolymers takes place at a higher temperature (350-600 °C) with lower weight loss (40%). These results indicate that BBE biopolymers are more stable than the non-crosslinked BHNC. This shows that the stability of BHNC increases after modification with βCD. Among all TGA curves, that of BBE1/1 is the most stable, indicating that the highest content of βCD has the largest effect on the hydrothermal stability of the biopolymers. This enhancement in thermal stability of BBE biopolymers could be due to the strong crosslinking interactions between the BHNC and βCD-EDA and serves as a thermal protective layer surrounding the BHNC particles, which enables this material to be used in high-temperature applications. Basically, differences could only be found in the thermal stability of the biopolymers. When comparing TGA curves of BBEs to that of BHNC, it can be concluded from the weight loss that βCD was successfully grafted on the surface of BHNCs.

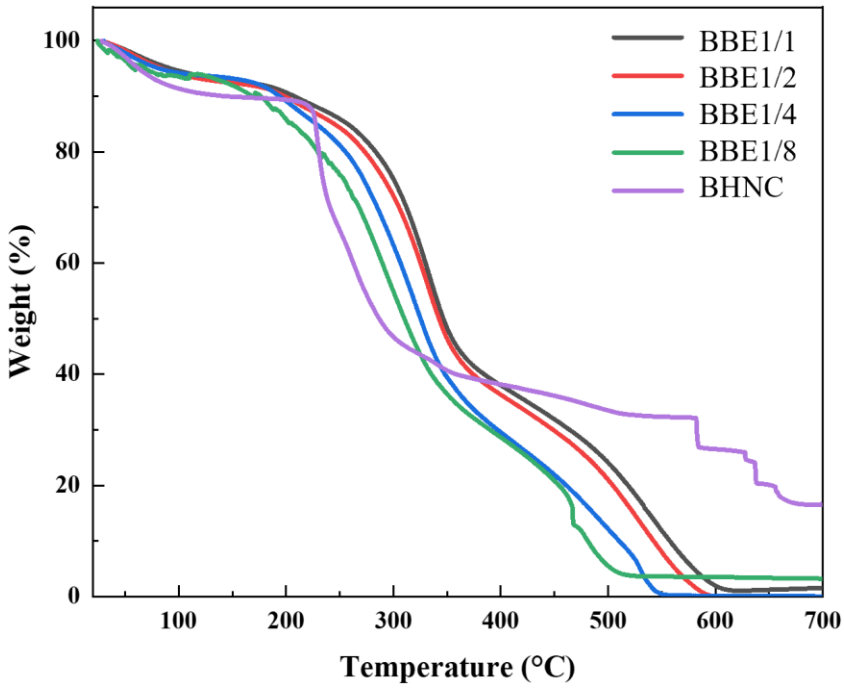

Figure 6. TGA of BHNC and trifunctional BBE biopolymers.

Characterization by BET analysis

In order to characterize the drug loading and release potential of the different BBE morphologies it is important to measure the surface area, pore size and, pore volume as these structures have unique porosity. N_2 adsorption-desorption isotherms were obtained to determine the pore size distribution and the surface of the different BBE polymers area, the results of which are shown in Figure 7. The surface area, pore size, and pore volume results are summarized in Table 1. From the BET plots, the BET equation yielded a pronounced decline of the surface area (determined from slope and intercept of linear BET plots in Fig.7) from 533 m^2/g in BHNC to 39-300 m^2/g in BBE, confirming the functionalization of βCD-EDA on BHNC. The decrease shows that the BHNC particles are not present as individual particles within the BBE matrix, but must be in a dense aggregated form. The various BBE polymers have 1-3 nm pores present in all the structures, presumably related to the βCD cavity that has a width of approximately 0.8 nm.

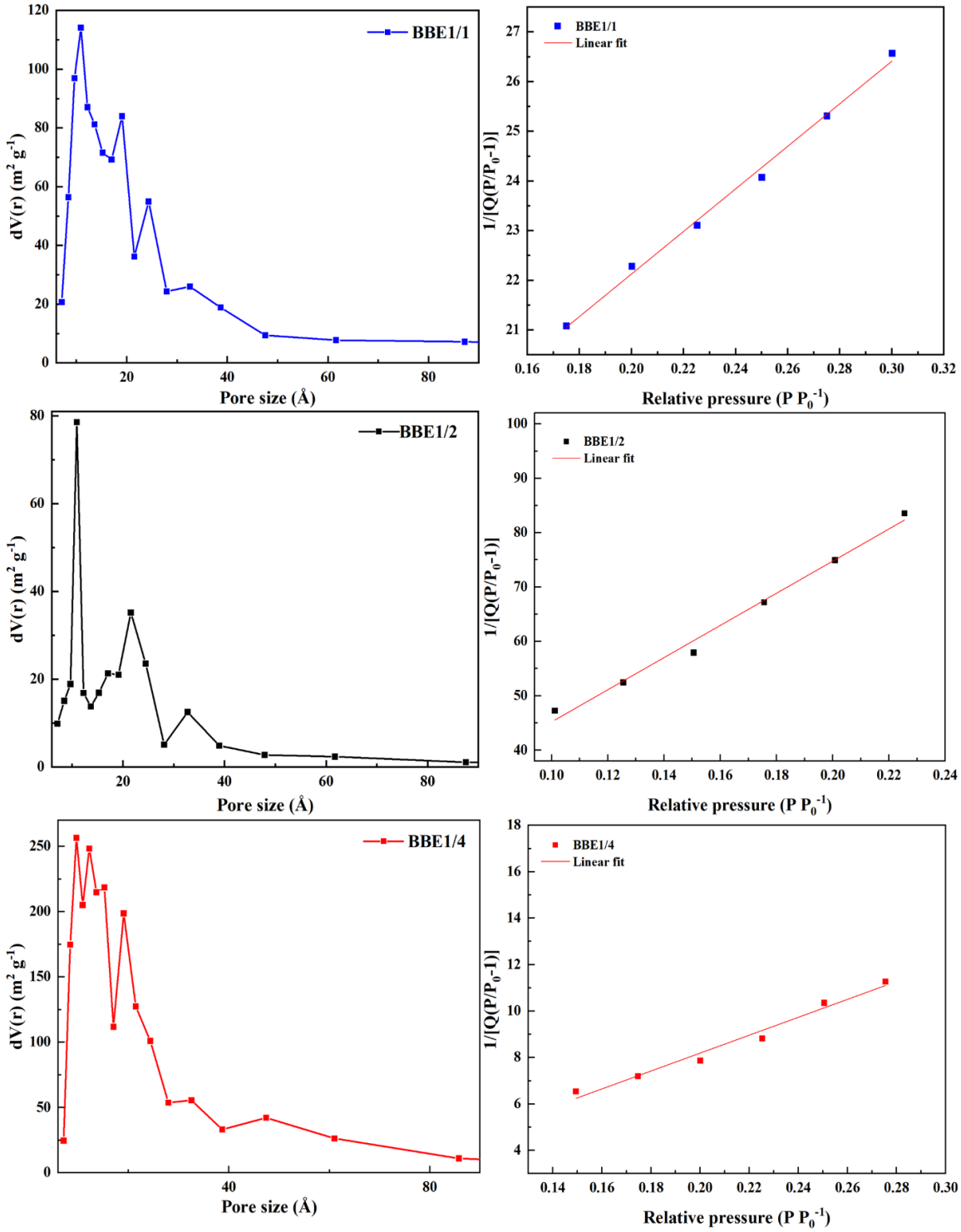

Figure 7. Pore size distribution of various BBEs (left) and corresponding linear BET plots (right), from which the specific surface area can be determent from the slope and intercept.

550

Table 1. Physiochemical properties of BHNC and the different BBE polymers.

Sample	Charge content (mmol/g)	Average size (nm)	Polydispersity	Surface area (m^2/g)	Pore volume (cm^3/g)	Average pore size (Å)	Zeta potential (in PBS solution) (mV)		
							pH 5.5	pH 6.5	pH 7.6
βCD-EDA	6	-	-	-	-	-	-	-	2.31
BHNC	4.5	138	0. 21	533*	-	-	-14	-18	-20
BBE1/1	0	1583	0.30	116	0.17	22	-4[#]	-7[#]	-9[#]
BBE1/2	2.25	1200	0.28	39	0.05	29	-9	-11	-12
BBE1/4	3.48	515	0.22	271	0.29	38	-10	-12	-16
BBE1/8	3.94	202	0.13	-	-	-	-13	-16	-20

Notes: *Calculated assuming cylindrical nanoparticles of 5 nm diameter and density of 1.5 cm^3/g.

[#]Negative zeta potentials for BBE1/1 are likely due to the adsorption of anionic impurities, which is almost unavoidable for neutral colloids. The same is observed for SNCC (sterically stabilized nanocrystalline cellulose)[47].

551

NMR spectroscopy

Structural characterization of all compounds was performed via NMR spectroscopy and the spectra obtained are shown in figure 8 and figure S9-11. The liquid ^{1}H NMR spectrum of pure βCD shows the characteristic peaks at 4.99, 3.89, 3.77, 3.79, 3.57, and 3.51 ppm corresponding to the H_1, H_3, H_5, H_6, H_2, and H_4 respectively (figure S9). Upon functionalization of βCD with CDI through hydroxyl groups of βCD, the peaks of βCD were observed and the peaks of carbonyl imidazole (CI) attached to βCD was observed with the characteristic peaks at 7.85, 7.23, and 6.86 ppm for hydrogen atoms of imidazole and two sharp peaks at 7.74 and 7.04 ppm related to the released imidazole from the nucleophilic reaction between CDI and βCD which was trapped in to the βCD cavity (Figure 8b). After that, the imidazole leaving groups in βCD-CI, were substituted by EDA with the carbamate bond formation. The successful preparation of βCD-EDA was structurally validated with liquid ^{1}H and ^{13}C NMR, HSQC and HMBC spectra shown in figure 8a, d, e, and figure S10, respectively. Compared to the ^{1}H NMR spectrum of βCD, βCD-EDA had new peaks at 2.6 and 3.1 for hydrogens of ethylene in EDA (figure 8a). On the other hand, these characteristic peaks were observed at 40 and 42.76 ppm (C_8 and C_9) in the ^{13}C NMR of βCD-EDA (figure 8d). Even more evidence for the successful grafting of βCD on EDA comes from ^{1}H, ^{13}C NMR, HSQC and HMBC. After attaching the EDA to βCD through the βCD-CI of the carbamate bond, peak shifts could be detected due to the functionalization of one C_6 of βCD, namely, a downfield shift of C_6 from 60.1 to 63.73 ppm, as well as upfield shifts of the adjacent C_5 from 73 to 70 ppm and C_1 from 102.1 to 101.9 ppm. These values are in accordance with the literature[46] which shows that the preparation of carbamate bonds with participation of hydroxyl groups on C_6 leads to a downfield shift of the carbon carrying the hydroxyl (C_6), a small upfield shift of the carbon C_5 as well as an even smaller upfield shift of the carbon C_1. The carbonyl of carbamate located at 158

ppm also shows that decorating βCD with EDA has clearly occurred. Moreover, the ^{1}H NMR spectrum of βCD-EDA (Figure 8a) showed new characteristic peaks of diastereotopic hydrogens on $C_{6'}$ ($H_{6'a}$ and $H_{6'b}$) at 4.14 and 4.38 ppm, and on $H_{5'}$ at 3.97 ppm. For accurate evaluation of these new peaks, the two-dimensional (2D) HSQC ^{13}C-^{1}H plot has been taken at 80 °C depicted in Figure 8e. One of the great advantages of HSQC compared to ^{13}C NMR and ^{1}H NMR is the determination of proton-carbon single bond correlations. From this diagram, a detailed interpretation of these protons is provided: firstly, both hydrogens at 4.1 and 4.4 ppm were correlated with the same carbon ($C_{6'}$ at 133 ppm), therefore, the two diastereotopic protons belong to a methylene group which is attached to the carbamate bond. Secondly, another new hydrogen peak at 4.0 ppm was correlated with $C_{5'}$ at 70 ppm implying that EDA was grafted on βCD. The $H_{6'a,6'b}$ chemical shift changes further prove that the reaction position was 6-OH. This result indicated that βCD reacted with EDA by forming the carbamate bond. Comparing the area of $H_{6'a,6'b}$ to the area of H_1 allows us to determine that the degree of substitution of βCD with EDA, which was found to be 3.5. This value is in consistent with the amide content of βCD-CI (3.2 mmoL/g obtained by titration (Figure S3)). Finally, the successful preparation of bio-derived BHNC-βCD-EDA (BBEs) trifunctional polymerized nanosponges and supramolecular inclusion complexes with DOX were observed in ^{13}C CP/MAS NMR spectra, illustrated in Figure 8c. In our previous work[32], the solid ^{13}C NMR spectrum revealed the expected pulp cellulose peaks of 105 ppm for (C_1), 85 and 90 ppm for (C_4), 80-70 ppm for (C_2, C_3, C_5), and 70-60 ppm for (C_6). Oxidation of pulp to DAMC fibers was confirmed by a broad peak at 85-105 ppm without any 170 ppm (carbonyl) peak suggesting the formation of hemiacetal groups. After oxidation of DAMC to BHNC the appearance of a new peak at 170-180 ppm (carboxylic acid) confirms the formation of BHNC and shows that the aldehyde peaks from DAMC were not completely lost. The region

between 50-110 ppm closely resembles that of cellulose, indicating that any remaining hemiacetal linkages were no longer observable after oxidation of DAMC. Compared to the BHNC spectrum, the presence of a new peak at 158 ppm, representing the carbamate groups and a new peak at 40 ppm due to the ethylene carbons in EDA are strong evidence that the BHNC building block particles were polymerized with βCD-EDA. Amide bonds which resulted from attaching amines from βCD-EDA to the activated carboxylic acid groups of BHNCs with the DMTMM activator overlap with the remaining carboxyl carbons and aldehyde carbonyls peaks in the BHNC spectrum. This broad peak is located at 170-178 ppm. The region 50-110 ppm closely resembles that of cellulose and βCD indicating that both bio-precursors are present. The inclusion complex of DOX-BBE has also been verified by comparing the solid-state ^{13}C CP/MAS NMR spectra of DOX-BBE and BBE (Figure 8c). Three sharp DOX characteristic peaks were present in the spectrum of DOX-BBE due to the carbon signal of aliphatic carbons in the DOX structure (17, 23, and 33 ppm). Moreover, multiple wide peaks around 50–110 ppm were observed corresponding to carbon signals of BBE. The peaks at 110, 119, and 134 ppm are ascribed to aromatic carbons corresponding to the DOX structure in the supramolecular inclusion complex and the new sharp peak at 187 ppm is related to the carbonyl of ketone in DOX, confirming the formation of supramolecular inclusion complex in βCD of BBE.

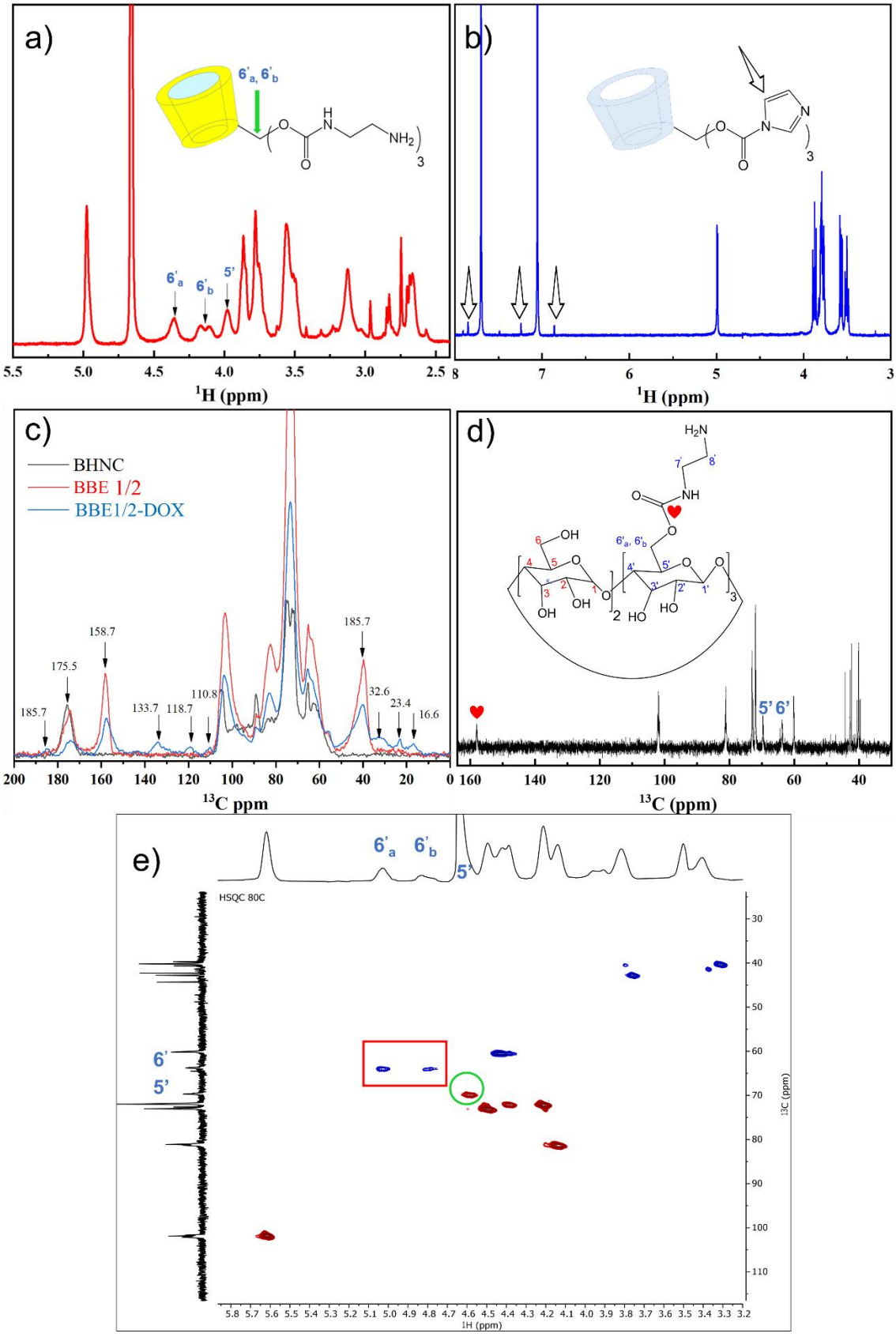
a)
6'a, 6'b
6'a
6'b
5'
1H (ppm)
b)
1H (ppm)
c)
BHNC
BBE 1/2
BBE1/2-DOX
185.7
175.5
158.7
133.7
118.7
110.8
185.7
32.6
23.4
16.6
13C ppm
d)
H2N
NH
OH
HO
5' 6'
13C (ppm)
e)
6'a 6'b
5'
HSQC 80C
6'
5'
1H (ppm)
13C (ppm)

Figure 8. a) ^{1}HNMR spectrum of βCD-EDA; b) ^{1}HNMR spectrum of βCD-CI; c) solid-state ^{13}C CP/MAS NMR of BHNC, BBE1/2 and BBE1/2-DOX; d) ^{13}C NMR spectra of βCD-EDA; (e) HSQC spectrum of βCD-EDA at 80 °C.

3.2. pH sensitive DOX loading and *in vitro* release of various BBEs

For the application of BBEs as biopolymer-based carriers, various BBEs were loaded with DOX to evaluate the effect of the polymer morphology, the ratio of bio-precursors, and the content of both BHNC and βCD on drug loading and release. UV spectrophotometry was used to characterize the loading and release of the doxorubicin from BHNC and the BBE polymers (Figure 9). The loading and release were examined at body temperature (37°C) under slightly acidic conditions (pH 5.5 and 6.5) that resemble tumor endosomal and lysosomal pHs, as well as at neutral blood pH 7.6, in order to estimate the effect of the tumor microenvironment on the release profile of DOX from the BBE polymers. The release behavior of DOX from BBEs directly influences the anticancer effect on the cancer cells. It is clear from Figure 9 that the loading capacity was higher for all BBE polymers compared to the BHNC control structure. Moreover, the absence of the cubic DOX morphology in the SEM images of the DOX-loaded biopolymers as well as the ^{13}C NMR results, proof that DOX is loaded in the supramolecular inclusion complexes of βCD and hence, we expect to see an increase in DOX loading capacity with increased βCD content, as observed. It appears that βCD enhances the loading by allowing DOX to be loaded in the βCD cavity and by allowing physisorption of DOX on the nanocellulose polymer matrix to occur. The release profiles of DOX-loaded BBEs (designated as BBE-DOX) with various morphologies were evaluated and the amount of DOX released is plotted in Figure 9 together with the release of DOX from BHNC. The release profile of DOX from BHNC suggests that there are two types of adsorbed molecules: those released very fast and those released very slowly. This is likely due to two different

adsorption mechanisms: possibly one due to ion-exchange, in which protonated DOX molecules act as counterions for the carboxyl groups in BHNC, and one due to physisorption. The counterions are released fast in the presence of a PBS buffer, whereas the physisorbed DOX molecules are released slowly. The effect of pH on DOX release from BHNC is counterintuitive. One would expect that more protonation of DOX at lower pH would increase the electrostatic attraction between DOX and carboxyl groups on BHNC, thus slowing down the release kinetics. However, the opposite is observed, implying that the physisorption of DOX on BHNC is not governed by electrostatics (scheme 6). The release profiles of BBEs, in which a certain amount of carboxyl groups is replaced by βCD-EDA cavities, are remarkably similar to those of BHNC. This is puzzling, as few or no counterions should be present in BBE1/1, implying the absence of ion-exchange. Taken in isolation, these profiles would imply the presence of weakly adsorbed DOX molecules and the adsorption of strongly adsorbed molecules, presumably in the βCD-EDA cavities. The comparison with BHNC suggests that DOX molecules adsorbed in βCD-EDA cavities are released at a similar rate as DOX molecules physiosorbed on BHNC. The pH dependence of the slow release of DOX from BBE can be due to the fact that at higher pH the DOX molecules are not protonated and from a stronger bond with the hydrophobic interior of the cavities. The weakly adsorbed DOX molecules are likely adsorbed on βCD-EDA, possibly due to hydrogen bonding between secondary amines in EDA and oxygen atoms in DOX. We confirmed that complex formation occurs between EDA and DOX by UV-vis (see Figure S12), which proves that DOX associates with EDA. With a decrease in βCD-EDA content, and an accompanied increase in carboxyl groups, the number of weakly adsorbed ions decreases and that of counterions increases, keeping the number of fast desorbing DOX molecules roughly equal (about 25%). The schematics of a plausible mechanism of DOX loading in BBEs and in BHNC as control, is shown

in scheme 6. From the mechanism one would expect that BBE1/1 has a much larger adsorption capacity than BHNC. Instead, the increase is only about 25%. This is like due to the extensive washing of the loaded sample, prior to measuring the DOX content, in which process most of the weakly adsorbing DOX molecules were removed.

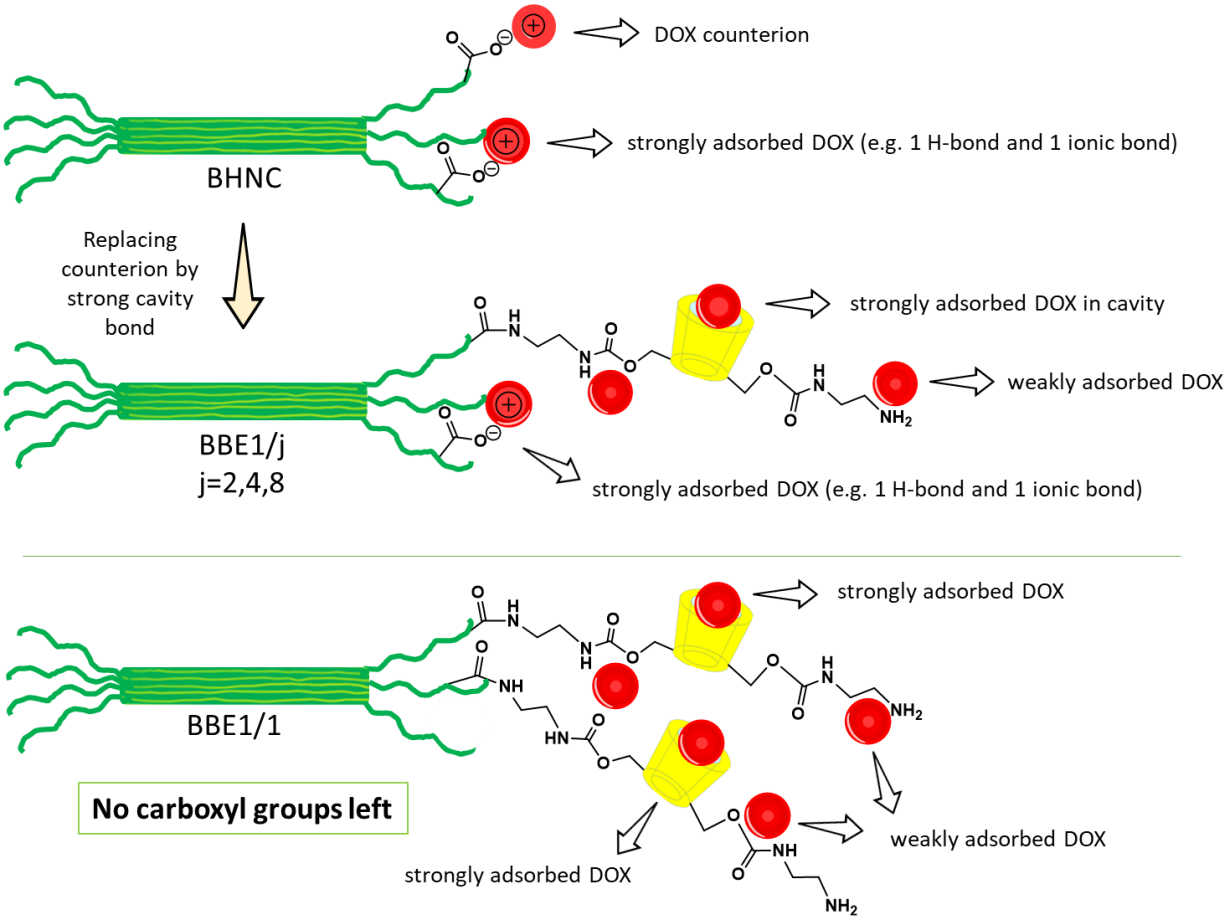

Scheme 6. Schematic illustration of strongly and weakly adsorbed DOX in BBE structures and BHNC.

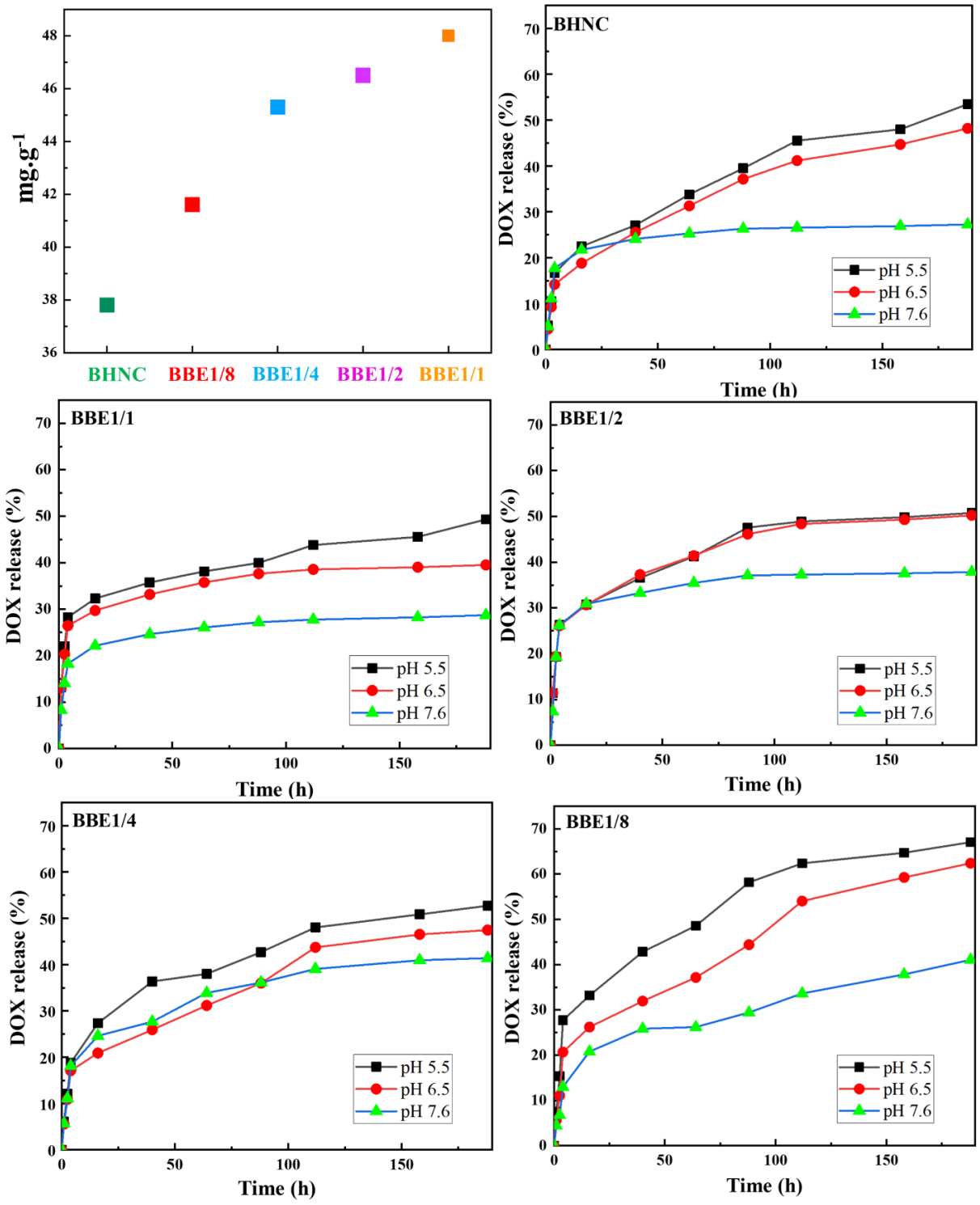

Figure 9. DOX loading capacity of BBE structures and BHNC and cumulative release profiles of DOX loaded-BBEs in pH 5.5, 6.5 and 7.4 PBS at 37 ℃.

3.3. Evaluation of the cytotoxicity of BBE-DOXs on human breast cancer cells

Biocompatibility of the BBE polymers was assessed using the metastatic chemo-resistant MDA-MB-231 breast cancer cell line that is widely used as a cancer cell model for drug screening due to its metastatic aggressiveness and chemoresistance. BBE1/1 and BBE1/4 were selected to be used as drug delivery bio-polymers in biological model MDA-MB-231 cells (Figure 10) since they represent soluble and insoluble BBE bio-polymers, respectively, and they did not have exaggerated DOX bursts especially, BBE1/4 with the fascinating helix structures. The reported IC50 for doxorubicin for MDA-MB-231 is 1.25 μM for 48 h incubation[48]. In our previous studies, we found that 5.04 μM doxorubicin was toxic for MDA-MB-231 cells at 24 h, we used this concentration for the toxicological assay. The cell viability was not significantly altered compared to control when DOX-free BBE bio-polymers were added, suggesting that they are biocompatible in vitro (Figure 10 b, c, and, Figure11). After 24 h of exposure, a significant decrement in cell viability was found in BBE-DOX and DOX samples compared with control. BBE1/4-DOX show more anticancer effect than free doxorubicin. The anticancer effect of BBE1/1-DOX with more loaded DOX was similar to BBE1/4-DOX. This is probably related to the helical structural that formed by capturing the liquid crystals of BHNC particles and water-soluble properties of this novel bio-polymer. Moreover, BBE1/4 has higher surface area, pore size and pore volume with compared to BBE1/1 which has a dense nanosponge structure, and hence βCD cavities in BBE1/4 are more accessible and more effective in releasing DOX. As a result, on average, BBE-DOX samples had a higher cytotoxicity than doxorubicin cultures, suggesting more anticancer effect than free doxorubicin. These BBE trifunctional bio-polymers as novel drug carriers can be used as remarkable structures for drug delivery with adjustable loading, release, and solubility.

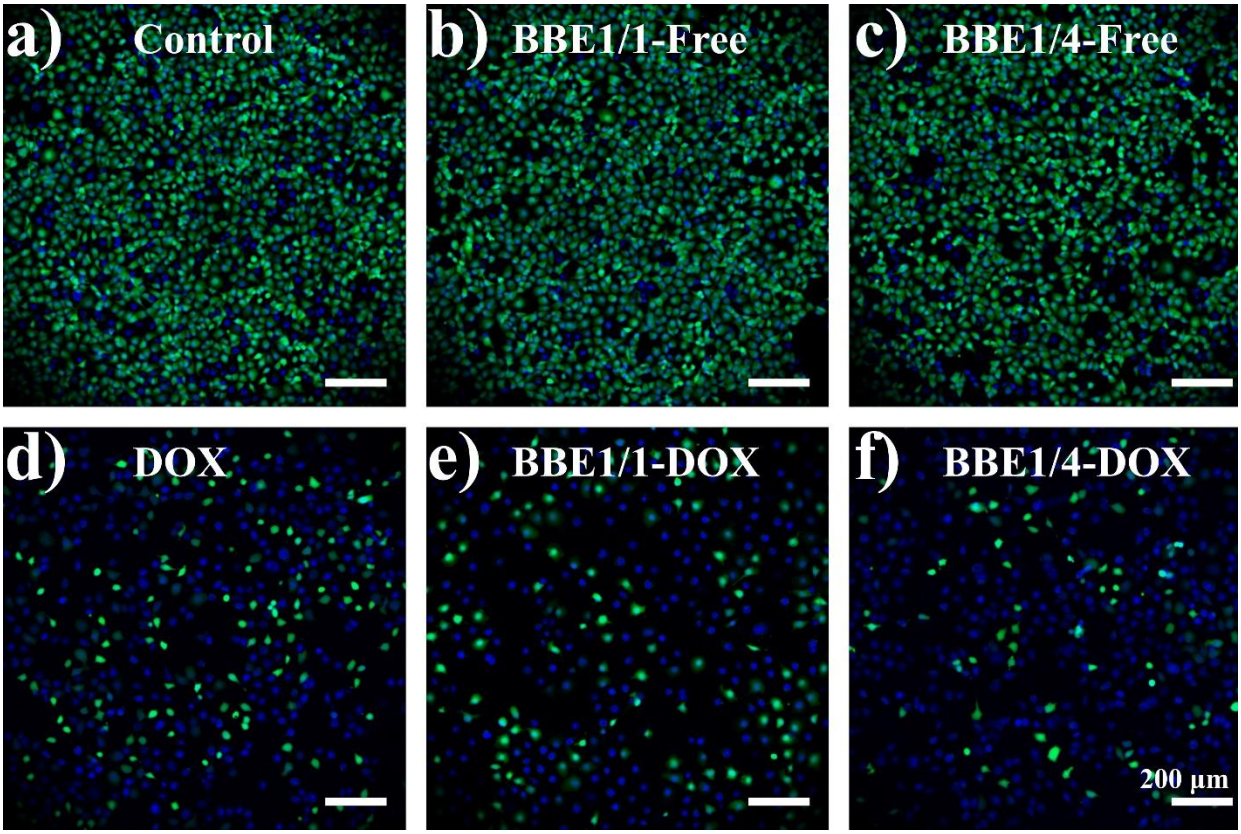

Figure 10. Confocal gallery of MDA-MB-231 exposed to BBE-DOX loaded. Breast cancer cells were incubated with BBE-Frees (b,c), BBE-DOXs (e,f), or DOX (d) for 24 h 5.04 µM (DOX-based concentration). Magnification ×10, scale bar 200 µm. Calcein-AM stains live cells as green; Hoechst stains nucleus of live and dead cells. MDA-MB-231 without nanomaterials were used as control (a).

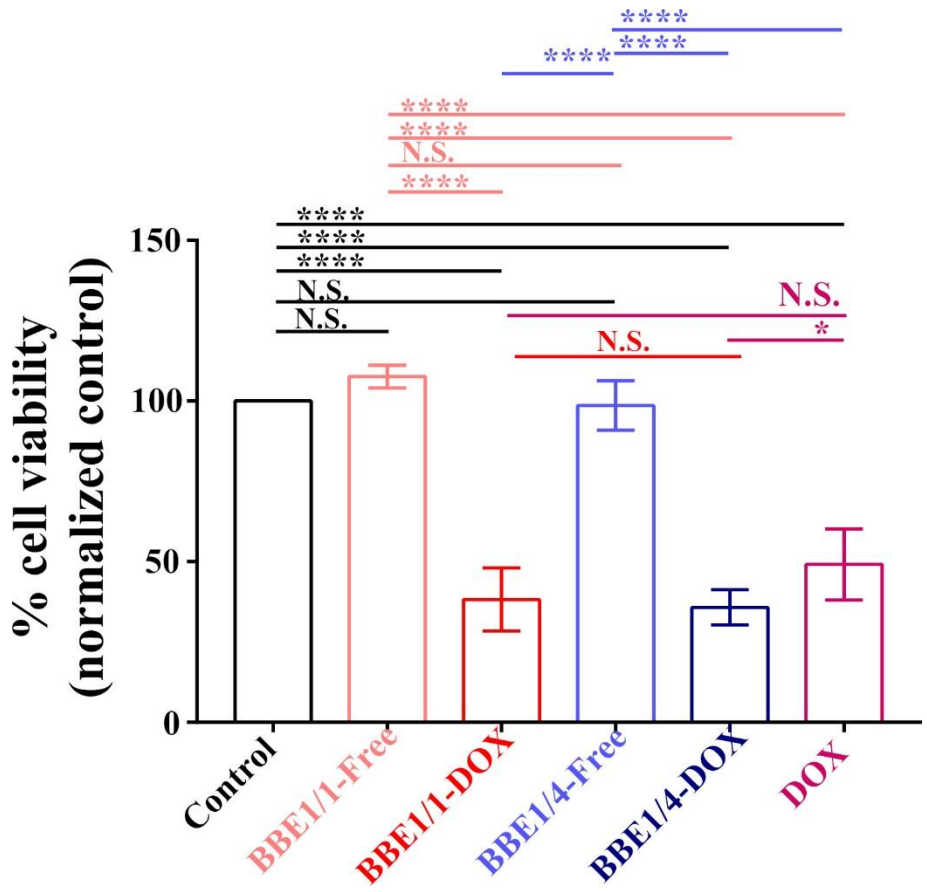

Figure 11. Viability of MDA-MB-231 exposed to BBE-Free, BBE-DOX, and DOX at 5.04 μM concentration of biopolymers loaded-doxorubicin or doxorubicin; data are presented as mean ± SD, n ≥ 3, *P < 0.05, ** P < 0.01, *** P < 0.001, **** P < 0.0001.

4. Conclusions

Novel and environmentally friendly bio-derived cellulose-beta cyclodextrin trifunctional anti-cancer carriers, BBEs, were fabricated via a facile one-pot and green synthesis by using βCD-EDA groups as cross-linkers. The objective was to determine the effectiveness of doxorubicin-loaded BBE against breast cancer cells. This system, based on the preparation of biopolymers with different morphology and novel DOX-loading and DOX-release behavior and characterization results, provides evidence that each component of BBEs has a crucial role in its functioning:

691 BHNC nanorods function as the backbone of this novel polymer; importantly, the βCD-EDA
692 groups play a role not only as cross-linkers but also a substrate for DOX molecules weakly
693 physisorbed on the tether (EDA) which links the cavity to the nanocellulose particles, and acting
694 as counterions for unreacted carboxyl groups. On the other hand, the DOX-loading and DOX-
695 release behavior mechanism of BBE is, after a burst of weakly adsorbed DOX, primarily due to
696 the host-guest inclusion complexation of immobilized βCD cavities. Moreover, these bio-based
697 hyper crosslinked polymers had a significant impact of DOX loading and DOX molecules could
698 be released effectively. The BBEs are biocompatible with cells, but the addition of doxorubicin
699 into their structure generates an attractive new drug delivery system with better outcomes than
700 doxorubicin alone enhancing the anticancer effects of DOX. These polymers have shown pH
701 responsiveness with enhanced release in acidic conditions which is very beneficial for passive
702 tumor targeting. Varying the grafting ratio of βCD-EDA on BHNC resulted in different polymers
703 with some different physiochemical properties, different morphologies, and different loading and
704 release profiles. Among the different polymers, the 1:4 crosslinking ratio (BBE1/4) resulted in
705 fascinating helical morphologies possibly due to the grafted βCD-EDA being optimum for
706 polymerizing liquid crystals of BHNCs stabilized in a polymer network. As a result, they had
707 enhanced anticancer effects in the breast cancer cell lines after they displayed high solubility in
708 water and high drug loading. More in-depth studies should be done to validate the effectiveness of
709 these new BBEs as drug carrier systems, including but not limited to: time-dose response, time-
710 dose drug releasing, applications on different cancer cell types, and more in vivo studies. This
711 study may lead to advancing practical applications of BBEs in drug delivery systems as they are
712 green, biocompatible, and versatile nanostructures with huge potential. Additionally, this work
713 adds a new insight to design and preparation of a trifunctional cyclodextrin-based polymer carriers,

which can be used for other drug delivery systems as well. It is believed that this green and ecofriendly cross-linking technology can be extended to prepare a wide variety of trifunctional materials for various applications.

Acknowledgements

The authors acknowledge the Natural Sciences and Engineering Research Council of Canada (NSERC-Discovery Grant 2018-05781) for supporting this research.

References

1. van der Zanden, S. Y.; Luimstra, J. J.; Neefjes, J.; Borst, J.; Ovaa, H., Opportunities for small molecules in cancer immunotherapy. *Trends in immunology* **2020**.

2. Huck, B. R.; Kötzner, L.; Urbahns, K., Small molecules drive big improvements in immuno-oncology therapies. *Angewandte Chemie International Edition* **2018,** *57* (16), 4412-4428.

3. Dextras, C.; Dashnyam, M.; Griner, L. A. M.; Sundaresan, J.; Chim, B.; Yu, Z.; Vodnala, S.; Lee, C.-C. R.; Hu, X.; Southall, N., Identification of Small Molecule Enhancers of Immunotherapy for Melanoma. *Scientific reports* **2020,** *10* (1), 1-11.

4. Samadi, P.; Saki, S.; Dermani, F. K.; Pourjafar, M.; Saidijam, M., Emerging ways to treat breast cancer: will promises be met? *Cellular Oncology* **2018,** *41* (6), 605-621.

5. Liu, T.; Song, S.; Wang, X.; Hao, J., Small-molecule inhibitors of breast cancer-related targets: Potential therapeutic agents for breast cancer. *European Journal of Medicinal Chemistry* **2020**, 112954.

6. Glassman, P. M.; Muzykantov, V. R., Pharmacokinetic and pharmacodynamic properties of drug delivery systems. *Journal of Pharmacology and Experimental Therapeutics* **2019,** *370* (3), 570-580.

7. Liu, S.; Dong, W.; Zeng, X.; Guo, Z.; Zong, P.; Li, B.; Meng, X.; Zuo, G., β-cyclodextrin modified g-C3N4 nanosheet: a fluorescent drug carrier with ultrahigh drug loading capacity and pH-responsive release. *Journal of Chemical Technology & Biotechnology* **2019,** *94* (2), 628-633.

8. Yu, M.; Xue, Y.; Ma, P. X.; Mao, C.; Lei, B., Intrinsic ultrahigh drug/miRNA loading capacity of biodegradable bioactive glass nanoparticles toward highly efficient pharmaceutical delivery. *ACS applied materials & interfaces* **2017,** *9* (10), 8460-8470.

9. Zhao, Z.; Ukidve, A.; Kim, J.; Mitragotri, S., Targeting strategies for tissue-specific drug delivery. *Cell* **2020,** *181* (1), 151-167.

10. Zhang, R.; Qin, X.; Kong, F.; Chen, P.; Pan, G., Improving cellular uptake of therapeutic entities through interaction with components of cell membrane. *Drug Delivery* **2019,** *26* (1), 328-342.

11. Shen, S.; Wu, Y.; Liu, Y.; Wu, D., High drug-loading nanomedicines: progress, current status, and prospects. *International journal of nanomedicine* **2017,** *12*, 4085.

12. Foss Hansen, S.; Larsen, B. H.; Olsen, S. I.; Baun, A., Categorization framework to aid hazard identification of nanomaterials. *Nanotoxicology* **2007,** *1* (3), 243-250.

13. Kuka, S.; Hurbánková, M.; Drlicková, M.; Baska, T.; Hudecková, H.; Tatarková, Z., Nanomaterials-a new and former public health issue. The case of Slovakia. *Central European journal of public health* **2016,** *24* (4), 308.

14. Berkner, S.; Schwirn, K.; Voelker, D., Nanopharmaceuticals: tiny challenges for the environmental risk assessment of pharmaceuticals. *Environmental toxicology and chemistry* **2016,** *35* (4), 780-787.

15. Dasmahapatra, A. K.; Dasari, T. P.; Tchounwou, P. B., Graphene-based nanomaterials toxicity in fish. *Reviews of Environmental Contamination and Toxicology Volume 247* **2018**, 1-58.

16. Quik, J. T.; Lynch, I.; Van Hoecke, K.; Miermans, C. J.; De Schamphelaere, K. A.; Janssen, C. R.; Dawson, K. A.; Stuart, M. A. C.; Van De Meent, D., Effect of natural organic matter on cerium dioxide nanoparticles settling in model fresh water. *Chemosphere* **2010,** *81* (6), 711-715.

17. Kiser, M. A.; Ryu, H.; Jang, H.; Hristovski, K.; Westerhoff, P., Biosorption of nanoparticles to heterotrophic wastewater biomass. *Water research* **2010,** *44* (14), 4105-4114.

18. Elsaesser, A.; Howard, C. V., Toxicology of nanoparticles. *Advanced drug delivery reviews* **2012,** *64* (2), 129-137.

19. George, A.; Shah, P. A.; Shrivastav, P. S., Natural biodegradable polymers based nano-formulations for drug delivery: A review. *International journal of pharmaceutics* **2019,** *561*, 244-264.

20. Nabipour, H.; Hu, Y., Sustainable drug delivery systems through green nanotechnology. *Nanoengineered Biomaterials for Advanced Drug Delivery* **2020**, 61.

21. Jana, P.; Shyam, M.; Singh, S.; Jayaprakash, V.; Dev, A., Biodegradable Polymers in Drug Delivery and Oral Vaccination. *European Polymer Journal* **2020**, 110155.

22. Kanwar, R.; Rathee, J.; Salunke, D. B.; Mehta, S. K., Green nanotechnology-driven drug delivery assemblies. *ACS omega* **2019,** *4* (5), 8804-8815.

23. Desai, A. G.; Qazi, G. N.; Ganju, R. K.; El-Tamer, M.; Singh, J.; Saxena, A. K.; Bedi, Y. S.; Taneja, S. C.; Bhat, H. K., Medicinal plants and cancer chemoprevention. *Current drug metabolism* **2008,** *9* (7), 581-591.

24. Laurén, P.; Paukkonen, H.; Lipiäinen, T.; Dong, Y.; Oksanen, T.; Räikkönen, H.; Ehlers, H.; Laaksonen, P.; Yliperttula, M.; Laaksonen, T., Pectin and mucin enhance the bioadhesion of drug loaded nanofibrillated cellulose films. *Pharmaceutical research* **2018,** *35* (7), 1-14.

25. Tan, T. H.; Lee, H. V.; Dabdawb, W. A. Y.; Abd Hamid, S. B. B. O., A review of nanocellulose in the drug-delivery system. *Materials for Biomedical Engineering* **2019**, 131-164.

26. Truong, N. P.; Whittaker, M. R.; Mak, C. W.; Davis, T. P., The importance of nanoparticle shape in cancer drug delivery. *Expert opinion on drug delivery* **2015,** *12* (1), 129-142.

27. Geng, Y.; Dalhaimer, P.; Cai, S.; Tsai, R.; Tewari, M.; Minko, T.; Discher, D. E., Shape effects of filaments versus spherical particles in flow and drug delivery. *Nature nanotechnology* **2007,** *2* (4), 249.

28. Toy, R.; Peiris, P. M.; Ghaghada, K. B.; Karathanasis, E., Shaping cancer nanomedicine: the effect of particle shape on the in vivo journey of nanoparticles. *Nanomedicine* **2014,** *9* (1), 121-134.

29. Heidari Nia, M.; Koshani, R.; Munguia-Lopez, J. G.; Kiasat, A. R.; Kinsella, J. M.; van de Ven, T. G. M., Biotemplated Hollow Mesoporous Silica Particles as Efficient Carriers for Drug Delivery. *ACS Applied Bio Materials* **2021**.

30. Yang, H.; van de Ven, T. G. M., Preparation of hairy cationic nanocrystalline cellulose. *Cellulose* **2016,** *23* (3), 1791-1801.

31. Yang, H.; Sheikhi, A.; van de Ven, T. G. M., Reusable green aerogels from cross-linked hairy nanocrystalline cellulose and modified chitosan for dye removal. *Langmuir* **2016,** *32* (45), 11771-11779.

32. Nia, M. H.; Tavakolian, M.; Kiasat, A. R.; van de Ven, T. G. M., Hybrid aerogel nanocomposite of dendritic colloidal silica and hairy nanocellulose: an effective dye adsorbent. *Langmuir* **2020,** *36* (40), 11963-11974.

33. Cova, T. F.; Murtinho, D.; Pais, A. A.; Valente, A. J., Combining cellulose and cyclodextrins: fascinating designs for materials and pharmaceutics. *Frontiers in chemistry* **2018,** *6*, 271.

34. Xia, D.; Wang, P.; Ji, X.; Khashab, N. M.; Sessler, J. L.; Huang, F., Functional supramolecular polymeric networks: the marriage of covalent polymers and macrocycle-based host–guest interactions. *Chemical Reviews* **2020,** *120* (13), 6070-6123.

35. Cova, T. F.; Murtinho, D.; Aguado, R.; Pais, A. A.; Valente, A. J., Cyclodextrin Polymers and Cyclodextrin-Containing Polysaccharides for Water Remediation. *Polysaccharides* **2021,** *2* (1), 16-38.

36. Gao, Y.; Guo, R.; Feng, Y.; Zhang, L.; Wang, C.; Song, J.; Jiao, T.; Zhou, J.; Peng, Q., Self-assembled hydrogels based on poly-cyclodextrin and poly-azobenzene compounds and applications for highly efficient removal of bisphenol A and methylene blue. *ACS omega* **2018,** *3* (9), 11663-11672.

37. Sarfraz, R. M.; Ahmad, M.; Mahmood, A.; Akram, M. R.; Abrar, A., Development of β-cyclodextrin-based hydrogel microparticles for solubility enhancement of rosuvastatin: an in vitro and in vivo evaluation. *Drug design, development and therapy* **2017,** *11*, 3083.

38. Krabicová, I.; Appleton, S. L.; Tannous, M.; Hoti, G.; Caldera, F.; Rubin Pedrazzo, A.; Cecone, C.; Cavalli, R.; Trotta, F., History of Cyclodextrin Nanosponges. *Polymers* **2020,** *12* (5), 1122.

39. Morin-Crini, N.; Crini, G., Environmental applications of water-insoluble β-cyclodextrin–epichlorohydrin polymers. *Progress in Polymer Science* **2013,** *38* (2), 344-368.

40. Li, H.; Meng, B.; Chai, S.-H.; Liu, H.; Dai, S., Hyper-crosslinked β-cyclodextrin porous polymer: an adsorption-facilitated molecular catalyst support for transformation of water-soluble aromatic molecules. *Chemical science* **2016,** *7* (2), 905-909.

41. Selvamuthukumar, S.; Anandam, S.; Krishnamoorthy, K.; Rajappan, M., Nanosponges: A novel class of drug delivery system-review. *Journal of Pharmacy & Pharmaceutical Sciences* **2012,** *15* (1), 103-111.

42. Yousef, T.; Hassan, N., Supramolecular encapsulation of doxorubicin with β-cyclodextrin dendrimer: in vitro evaluation of controlled release and cytotoxicity. *Journal of Inclusion Phenomena and Macrocyclic Chemistry* **2017,** *87* (1), 105-115.

43. Yang, C.; Huang, H.; Ji, T.; Zhang, K.; Yuan, L.; Zhou, C.; Tang, K.; Yi, J.; Chen, X., A cost-effective crosslinked β-cyclodextrin polymer for the rapid and efficient removal of micropollutants from wastewater. *Polymer International* **2019,** *68* (4), 805-811.

44. Guerra, F. D.; Attia, M. F.; Whitehead, D. C.; Alexis, F., Nanotechnology for environmental remediation: materials and applications. *Molecules* **2018,** *23* (7), 1760.

45. Zhang, F. Synthesis of β-Cyclodextrin Functionalized Cellulose Nanocrystals and Their Interactions with Amphiphilic Compounds. University of Waterloo, 2014.

46. Tang, B.; Liang, H.-l.; Tong, L.-l.; Li, P., Synthesis of ethylenediamine linked β-cyclodextrin dimer and its analytical application for tranilast determination by spectrofluorimetry. *Bioorganic & medicinal chemistry* **2006,** *14* (11), 3947-3952.

47. Yang, H; Chen, D. van de Ven, T. G .M. *Cellulose* **2015,** *22*, 1743–175 .

48. Wen, S.-h.; Su, S.-c.; Liou, B.-h.; Lin, C.-h.; Lee, K.-r., Sulbactam-enhanced cytotoxicity of doxorubicin in breast cancer cells. *Cancer cell international* **2018,** *18* (1), 1-18.